The Hemodynamics of Native and Surgical Aortic Valves with regards to Wall Shear Stress and Residence Time.

Thesis by

Alexandros Yiannis Rosakis

In Partial Fulfillment of the Requirements for

the degree of

Doctor of Philosophy

CALIFORNIA INSTITUTE OF TECHNOLOGY

Pasadena, California

2023

Defended August 25, 2022

© 2022

Alexandros Y Rosakis
ORCID: 0000-0001-9170-1002

ACKNOWLEDGEMENTS

I do not think that I will ever be able to properly express the depth of my gratitude to those who have supported me, but I will try.

First, I would like to thank my research advisor, Mory Gharib. It has been a long time since the start of my journey in his lab as an undergraduate summer intern and every moment has helped me grow as a researcher and as a person. Without his guidance and encouragement, none of my work would have been possible.

I thank my thesis committee, Guruswami Ravichandran, Mikhail Shapiro, and Manoochehr Koochesfahani, for their support and advice during my time as a graduate student.

I would like to thank all of the past and present members of the Gharib Group. I could not have asked for a better group of lab mates and friends. I have learned so much from all of you and you have made it a joy to come into the office every day.

I thank Jason Beith. He has shared a wealth of knowledge and experience that would be impossible to find anywhere else. My conversations with him helped shape my work and he always brought a positive outlook that helped me through the rough times.

I thank all of the dear friends I have met along the way, including Noah, Varun, and Vince, among so many others. I know that I could not have made it through without your love and support. I have been truly blessed to have met you.

I thank my girlfriend, Jessica. I am immeasurably happy that you have put up with me throughout grad school, through both the bad and the good. You have made every day so much better.

Finally, I would like to thank my family. To my parents, Ioanna and Ares, everything I have accomplished and the person I am today is a credit to you. You have loved and supported me my entire life and no amount of thanks can express how lucky I feel. To my siblings, Angele and Phillip, and my nieces and nephew. I love you all dearly and I am so happy that we will finally be living in the same city soon.

ABSTRACT

Cardiovascular diseases are the leading causes of illness and death all around the world. The third most common cardiovascular disease is aortic stenosis (AS). AS is most commonly characterized as a stiffening of the native trileaflet aortic valve, which impedes blood flow into the aorta and puts extra stress on the heart. The aorta is the main artery that supplies oxygenated blood to the body. AS has been widely studied in the past. However, there has been little work in understanding the complex effects that non uniform stiffening of the aortic valve can have on the hemodynamics inside the aorta.

The most effective treatment for AS is to replace the stiffened valve with a prosthetic valve. Care must be taken to ensure that the replacement actually performs better hemodynamically. A major metric for prosthetic valve performance is the transvalvular pressure drop which is a measure of how much pressure, and energy, is lost as the heart pumps blood through the valve. Generally speaking, larger valves exhibit a smaller pressure drop because they restrict the flow to a lesser degree. This phenomenon has led to a trend for surgeons to implant the largest prosthetic valve possible, and in some cases, to expanding the aorta to fit even larger valves. However, there has been relatively little work done on determining the effects of valve oversizing on the blood flow inside the Aorta.

The aims of this study were two-fold. First, a model of AS was tested inside an *in vitro* aortic simulator in order to identify how different individual leaflet stiffnesses would affect blood flow. Digital particle image velocimetry (DPIV) was used to measure velocity profiles inside a model aorta. The DPIV results were used to estimate the wall shear stress and blood residence time. Our analysis suggests that leaflet asymmetry greatly affects the amount of WSS by vectoring the systolic jet and that stiffened leaflets have an increased residence time. This study indicates that valve leaflets with different stiffness conditions can have a more significant impact on wall shear stress than stenosis caused by the uniform increase in all three leaflets (and the subsequent increased systolic velocity) alone. Second, the experimental apparatus was used to test different prosthetic valve sizes and valve mounting methods in order to identify how they affected residence time inside the sinus bulge. Dye

residence experiments and DPIV were used to measure fluid stasis in several different combinations of prosthetic valve sizes, sinus sizes, and valve mounting methods. Our results indicate that valve to sinus sizing and mounting method is very important and can lead to greatly increased residence time and thrombosis risk. We have also identified a metric that can predict the threshold at which valves become oversized.

PUBLISHED CONTENT AND CONTRIBUTIONS

Rosakis, Alexandros, and Morteza Gharib. “The Influence of Valve Leaflet Stiffness Variability on Aortic Wall Shear Stress.” Annals of Biomedical Engineering, vol. 50, no. 1, 2022, pp. 29–38., doi:10.1007/s10439-021-02899-5.

A. Rosakis participated in the conception of the project, setting up the experiment, analyzing the data, and the writing of the manuscript.

TABLE OF CONTENTS

Acknowledgements……...iii
Abstract ……iv
Published Content and Contributions…….....vi
Table of Contents……vii
List of Illustrations and/or Tables……viii
Chapter I: Introduction 1
1.1 The Heart 1
1.2 Aortic Stenosis and Wall Shear Stress 2
1.3 Prosthetic Aortic Valves and Blood Residence Time 4
Chapter II: Experimental Setup and Methods 7
2.1 Aortic Root Model 7
2.1.1 Native Valve Model 7
2.1.2 Prosthetic Valve Model 10
2.2 Dye Measurements 12
2.3 PIV Measurements 13
2.4 Wall Shear Stress Measurements 14
2.5 Residence Time Measurements 16
Chapter III: Results 18
3.1 Native Valve Leaflet Stiffness Asymmetry 18
3.1.1 Qualitative Flow Measurements 18
3.1.1 Systole Velocity Profiles 19
3.1.2 Wall Shear Stress 21
3.1.3 Residence Time 23
3.2 Prosthetic Valve Hemodynamics 23
3.2.1 Valve Sizing 23
3.2.2 Mounting Geometry 31
Chapter IV: Discussion 37
4.1 Native Valve Leaflet Asymmetry 37
4.2 Prosthetic Valve Hemodynamics 38
4.3 Limitation 42
Bibliography 45
Appendix A: 50

LIST OF ILLUSTRATIONS AND/OR TABLES

Number *Page*

1.1 The Heart 2
1.2 Prosthetic Aortic Valves 6
2.1 Experimental Setup 9
2.2 Stenotic Valve Configurations 10
2.3 Glass Aorta Models 12
2.4 Aorta Model Coordinate System 15
2.5 Residence Time Measurement Region 17
3.1 Particle Streak Visualization 19
3.2 Systolic Jet Profiles 21
3.3 WSS Distributions 22
3.4 Leaflet Residence Time 23
3.5 Dye Test Time Sequence: Valve Sizing 25
3.6 Dye Quantification: Valve Sizing 26
3.7 Dye Quantification: Polymer vs Bioprosthetic 26
3.8 Dye Quantification: Sinus Sizing 27
3.9 Average Velocity Heatmaps 28
3.10 Mixing Metrics Near the Leaflets 29
3.11 Mixing Metrics Near the Posts 30
3.12 Mixing Metrics in the Post Sinus Gap 31
3.13 Dye Test Time Sequence: Cor-Knots 32
3.14 Dye Quantification: 25 mm Perimount 33
3.15 Dye Quantification: 23 mm Tria 33
3.16 Dye Quantification: 21 mm Tria 34
3.17 Cor-Knot Mixing Metrics Near the Leaflets 35
3.18 Cor-Knot Mixing Metrics Near the Posts 35
3.19 Cor-Knot Average Velocity Heat Maps 36

4.1 Mixing Metrics vs Formation Gap Ratio Near the Posts 42

Chapter 1

Introduction

1.1 **The Heart**

The heart is the organ responsible for pumping blood throughout the human body. It is made up of four chambers: the left atrium, the left ventricle, the right atrium and the right ventricle (figure 1.1). The right side of the heart is dedicated to pumping deoxygenated blood through the pulmonary arteries and the lungs in order to replenish the blood's oxygen and remove carbon dioxide. The blood then is pumped through the pulmonary veins until it reaches the left atrium. The left atrium contracts and forces blood through the mitral valve and into the right ventricle. The contraction of the left ventricle increases the pressure inside the chamber and causes the mitral valve to close[2]. Once the pressure inside the left ventricle has increased to the point where it is equal to the pressure inside the aorta, the aortic valve opens. As the pressure inside the left ventricle further increases, the blood inside the ventricle is forced into the aorta[17]. The aorta is a major blood vessel that supplies oxygenated blood to the entire body. It is composed of three main parts: the ascending aorta, the aortic arch, and the descending aorta. The ascending aorta houses the sinus bulge (also commonly referred to as the aortic sinus or sinus of Valsalva) which is a widening of the aorta around the aortic valve. The aortic valve has three leaflets and is actuated passively, meaning that there is no active control that dictates whether the valve is open or closed and prevents liquid from entering the ventricle after contraction. For the purposes of this work, the cardiac cycle can be broken into two parts: systole, when the left ventricle contracts and blood is forced through the aortic valve, and diastole, when the aortic valve closes and the left ventricle refills with blood. The number of cardiac cycles per minute is referred to as the heart rate and is measured in beats per minute. The amount of fluid pumped out of the ventricle in each cycle is stroke volume (which is measured in milliliters). The product of the stroke volume and the heart rate is the cardiac output (measure in liters per minute) and is a measure of how much blood the heart is pumping at any given time.

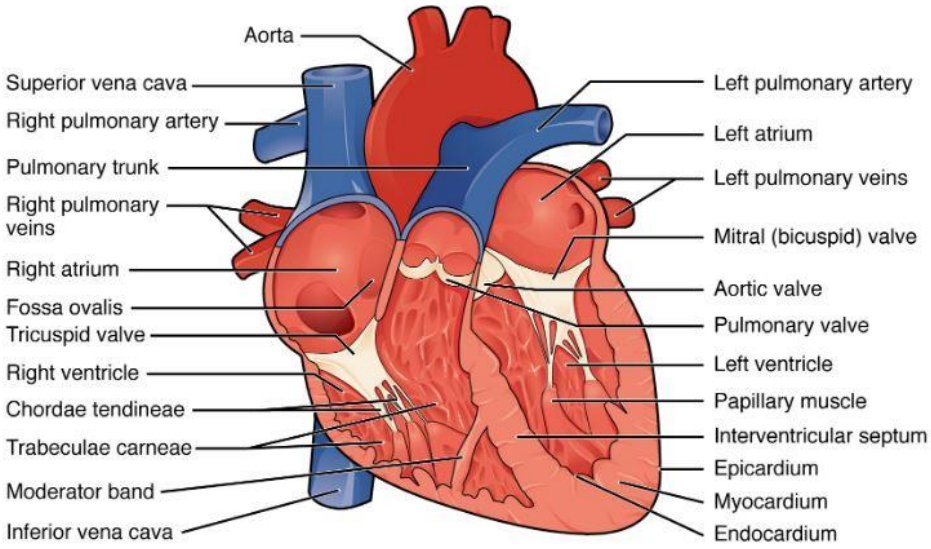

Figure 1.1 A schematic of the human heart and the major arteries and vein that connect to it. Adapted from https://openstax.org/books/anatomy-and-physiology/pages/19-1-heart-anatomy

1.2 **Aortic Stenosis and Wall Shear Stress**

Aortic Stenosis (AS) is the third most common cardiovascular disease in the world[37]. Aortic stenosis is characterized by a decrease in the effective orifice area of the tri-leaflet aortic heart valve. The primary effect of this condition is the restriction of blood flow from the heart because the left ventricle forces the blood through a smaller than normal valvular opening. Clinically, AS is commonly characterized through the American College of Cardiology (ACC)/American Heart Association (AHA) guideline[3]. This guideline sets criteria for the jet velocity, pressure gradient, and valve area and classifies stenosis into mild, moderate, and severe categories. There can be several mechanisms by which AS can occur, but the most common is the calcification of the aortic valve leaflets. Calcification effectively increases the stiffness of the leaflets[39] and prevents them from fully opening.

In addition to restricting blood flow into the aorta, the conditions mentioned above can create abnormal hemodynamics downstream of the valve. These irregular blood flows can arise

from asymmetrical stiffening of the valve leaflets, which can change the distribution of wall shear stress (WSS) in the ascending aorta[1]. Abnormal WSS can have several detrimental effects depending on the magnitude and frequency of the stress. Low and oscillatory WSS can lead to thrombus formation and atherosclerotic lesions[10]. High wall shear stress can lead to shear-induced thrombotic trauma[47]. Researchers have connected the eccentric systolic jets created by certain types of mechanical heart valves and bicuspid aortic valves to the growth of saccular aneurysms and increased WSS where the jets impinge on the aortic wall[31,36,42]. Furthermore, disrupting normal aortic hemodynamics and valve leaflet opening kinematics may affect the residence time near the leaflets. Residence time has previously been used to identify the risk of thrombus formation in the sinus bulge[20].

Previous studies have demonstrated that AS causes higher aortic WSS through in vitro experiments, in silico simulations[25], and in vivo observations[30,38]. The decrease in effective orifice area associated with AS causes velocity of the systolic jet to increase during each cardiac cycle as the heart attempts to maintain a specific cardiac output. The high velocity systolic jets increase the vorticity and turbulence in the ascending aorta[30] and impinge on the aorta leading to high shear and normal stresses[25]. However, existing studies typically model AS as a symmetric decrease in the effective orifice area of the aortic valve. While this simplification is useful for high level observations on the effects of AS, and for statistical analyses with clinical datasets, it does not capture the complex hemodynamics that occur downstream of individual stenotic valves. Computed tomography of AS valves shows the variance in calcium deposits between individual leaflets[34]. In some cases, singular leaflets can remain completely free from calcium deposits. Non-uniform stiffening of the stenotic valves, in effect, alters the valvular opening geometry and may lead to downstream hemodynamics similar to those created by the mechanical heart valves and bicuspid valves mentioned earlier [31,36,42].

The aforementioned work investigates the effect of aortic valve leaflet stiffness variability on the flow inside the ascending aorta and the distribution of WSS in a physiologically relevant in vitro model. The parameters measured include velocity profiles of the systolic

jets, WSS, and residence time. Valve modification was achieved by stiffening individual leaflets on a polymer prosthetic aortic valve. Various configurations of stiffened leaflets serve as a model for aortic valve stenosis.

1.3 **Prosthetic Aortic Valves and Blood Residence Time**

The only effective treatment for severe aortic stenosis is aortic valve replacement surgery [35] where a prosthetic valve replaces the stenotic native valve. There are several different types of prosthetic heart valves that fall into three main categories: mechanical valves, bioprosthetic valves, and polymer valves (Figure 1.2). Mechanical valves are valves that are constructed from manmade materials such as metals and plastics. Some examples of these include ball in cage valves, single leaflet, and bileaflet valves[8]. They exhibit excellent durability and often last for the entire lifespan of the patient. However, they require lifetime anticoagulation treatment because they are prone to thrombus formation[29]. Furthermore, these valves can create abnormal systolic jets that can affect the endothelial lining of the aorta as was described in the previous section. Bioprosthetic valves are created using biological tissue and mimic the shape of the native trileaflet aortic valve. They can be xenografts, which are created from either porcine or bovine tissue, or they can be homografts, which are donated human valves[8]. Bioprosthetic valves perform better hemodynamically, however they are typically less durable than mechanical valves and can calcify similarly to native valves[29]. Polymer valves, as the name would suggest, are created using a synthetic polymer to create compliant leaflets that mimic the shape of the native valve. The benefits of using a synthetic polymer for valve construction are numerous. Polymer valves would be much easier and cheaper to manufacture, would be resistant to biofouling, and would exhibit excellent hemodynamics on par with native and biological valves. At the time of writing, there is currently one polymer valve that is undergoing clinical trials[24]. This study will focus on bioprosthetic and polymer valves because the problematic hemodynamic performance of mechanical valves has been investigated by several researchers in the past[6,26,44]. However, to summarize, mechanical valves have been shown to cause cavitation, which can lead to blood cell damage. This increases the propensity for thrombus formation. Furthermore, some

mechanical valves can create highly eccentric systolic jets that have been theorized to cause aortic saccular formation, as was mentioned in the previous section.

Historically, prosthetic valve performance has been measured in a very similar way to AS. The effective orifice area of the valve normalized to the body surface area of the patient is used to determine whether the size of the valve is too small. In such cases, the patient is said to experience valve prosthesis-patient mismatch (PPM) [14,15]. The consequence of PPM is the generation of higher-than-normal transvalvular pressure gradients[40]. In essence, the smaller valve orifice area constricts the flow from the heart which causes the ventricle to have to work much harder to pump the same amount of blood. The transvalvular pressure gradient is a metric of how much energy is lost across the valve and typically decreases with larger effective orifice area and increases with higher flow rates. Large pressure gradients can lead to left ventricle hypertrophy and decreased survival rates after aortic valve replacement[15,32]. In order to avoid PPM and high transvalvular pressure gradients, surgeons tend to choose the largest size prosthetic valve that can be physically fit inside the sinus[9] and in some cases even surgically expanding the aortic root with a procedure known as patch enlargement so that larger valves could be implanted[43]. However, there has been very little work on the effects of deliberately oversizing prosthetic valves. The few studies that exist focus on how valve oversizing can physically deform prosthetic valves such that they do not open, hurting their hemodynamic performance[7,9].

The following work presents a discussion on the effect of geometrical factors such as valve sizing and valve mounting methods, such as Cor-knots, on the blood flow around the valve, specifically, regarding blood residence time. Residence time is a measure of blood stagnation and stasis. High residence time increases the risks of thrombus formation[12]. Thrombus formation inside the aorta can cause strokes or transient ischemic attacks[33]. It has also been shown previously that thrombus formation can occur on valves with improperly expanded leaflets[16] or geometric confinements due to valve in valve (VIV) procedures[46] (when a transcatheter valve is implanted inside a poorly performing preexisting prosthetic valve). Cor-Knots (LSI Solutions) are a surgical device that removes the need for manually tying

knots when suturing the valves to the aortic annulus. The Cor-Knot device leaves between 10-12 4-millimeter titanium posts protruding into the sinus bulge. Some examples of Cor-knots can be seen in Figure 1.2. They have been shown to reduce surgery times. However, there is an ongoing debate on whether they actually provide long term benefit to patients[23]. We theorize that the presence of Cor-Knots may reduce blood flow and increase residence time around the base of the valves.

In order to study the effects of geometrical factors such as Cor-Knots and valve sizing and their impacts on life threatening thrombosis risks, we performed several experiments. The parameters studied were dye residence time and several fluid washout metrics such as average flow velocity and velocity fluctuation deviation. Tests were performed in vitro with a model aorta and flow simulator that replicated the conditions inside a typical human aorta.

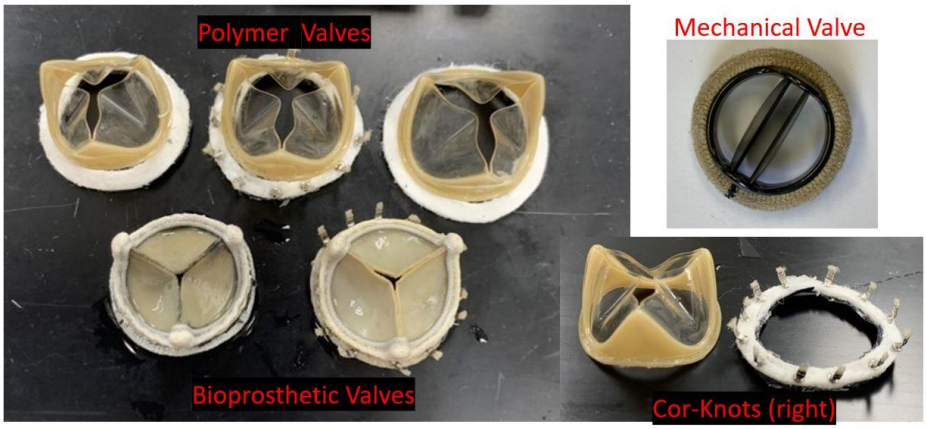

Figure 1.2: Examples of Mechanical valves, Bioprosthetic valves, and Polymer valves. Cor-Knots can also be seen on several of the sewing cuffs (most notable in the bottom right).

Chapter 2

Experimental Setup and Methods

This chapter describes the experimental setup used to simulate blood flow inside the aorta directly downstream of the aortic heart valve and the techniques implemented to measure the aforementioned flow.

2.1 **Aortic Root Model**

This section is dedicated to describing our in vitro test apparatus that lets us mimic the conditions inside the aorta during the complete cardiac cycle.

2.1.1 **Native Valve Model**

A schematic of experimental setup can be seen in figure 2.1. The native aortic valve and ascending aorta model was developed to closely approximate a typical human aorta. It was constructed with a polymer prosthetic tri-leaflet heart valve mounted to the base of a curved glass pipe with an internal diameter of 28 mm. Following the position of the heart valve, the diameter of the glass model widened to 34 mm to simulate the sinus bulge. Downstream of the sinus bulge, the pipe bent into an arc with a radius of curvature of 53mm. This portion acted as the ascending aorta and the aortic arch. A pulsatile heart pump (Harvard Apparatus) drove fluid through the valve with a stroke volume of 70 mL at 50 beats per minute (bpm). The duty cycle of the pump was set to 30% systole and 70% diastole. A water column connected to the end of the glass pipe provided physiological back pressure of 100 mmHg on the valve during diastole. The water column emptied into a reservoir heated to 37 degrees Celsius to simulate the average body temperature and ensure that the heart valve polymer functioned at its designed specifications. The entire aorta model was immersed into the reservoir to ensure uniform heating and to reduce the distortion caused by the index of refraction mismatch between the working fluid and the surrounding air. The fluid used for the native valve experiments was pure de-ionized water.

In this model, we used a tri-leaflet 23mm Tria polymer heart valve (courtesy of Foldax Inc.). The valve is constructed using Siloxane Poly(urethane-urea) Elastomer[24] which is touted to exhibit excellent biocompatibility and biostability while limiting risk of thrombus formation and calcium deposition. Additionally, the valve geometry mimics native trileaflet heart valves. Figure 2.2 shows a close-up of the prosthetic valve.

Four configurations of the prosthetic heart valve were tested (Figure 2.2). The first configuration was a typical polymer heart valve where no leaflets were stiffened. This case will be referred to as symmetric typical (ST) and measured as a baseline for standard heart valve operation. The second case was a polymer heart valve where all leaflets were stiffened. This fully stiffened configuration will be referred to as symmetric stenotic (SS) and modeled severe aortic valve stenosis. The third case was a polymer valve with a single stiffened leaflet. In this case, the stiffened leaflet was oriented near the inner wall of the aortic arch and will be referred to as asymmetric one (A1). The last case was a polymer valve with two stiffened leaflets. The stiffened leaflets were positioned near the outer wall of the aortic arch and will be referred to as asymmetric two (A2). The stiffening of leaflets was achieved by depositing several layers of Sylgard 184 Polydimethylsiloxane (PDMS) on each leaflet to increase their thickness from 0.05 mm to 0.5 mm. PDMS is an organic silicone compound that was deposited on the valve leaflets in a liquid form and then cured using the curing agent that came with the Sylgard kit. It was cured at 40 degrees Celsius, which created a silicone polymer with a Young's modulus of 1.5 MPa[27]. The material properties of native leaflets and calcium deposits vary, but we used a value of 6 MPa for the leaflet and a value of 1000 MPa for calcium deposits[4]. By thickening the leaflets by a factor of 10, we increased their effective stiffness by a factor of 1000 because stiffness is proportional to Young's modulus and to the cube of the thickness (for a thin plate). Therefore, stiffened leaflets exhibited a 1000-fold increase in stiffness versus the unstiffened leaflets and served as an adequate model of severely stenotic aortic valves. The PDMS could be peeled off to return the valve to its unmodified configuration.

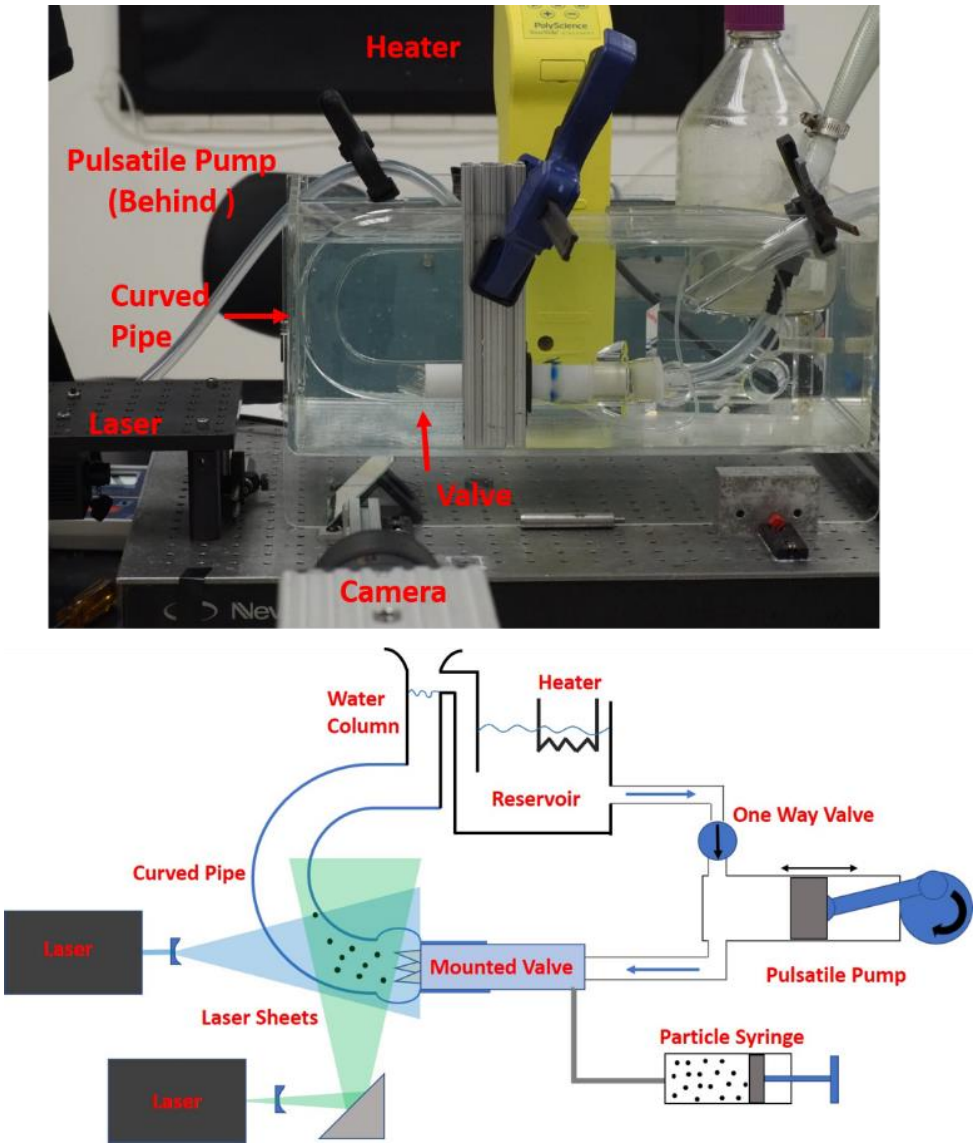

Figure 2.1: Top: Photograph of the experimental Setup. Note that the sinus bulge is missing in the curved glass pipe shown. Bottom: Schematic of the Experimental Setup. Note the laser sheets that were used to illuminate the DPIV particles. These laser sheets bisected the aortic arch and aortic valve. Care was taken to ensure that the laser sheet remained in the same location for every test.

Figure 2.2: 27mm Polymer Prosthetic Heart Valves developed by Foldax. Four different experimental configurations are shown where red overlays on the leaflets indicate that they have been stiffened from 0.05 mm to 0.5 mm

2.1.2 **Prosthetic Valve Model**

The glass aorta model described in the previous section was modified to allow for sinus bulges of varying diameters to be installed to study flow patterns of different diameter valves in a range of normally sized sinus bulges found in patients. The sinus bulge can range from 27 mm to 36 mm in human adults[13]. This was accomplished by cutting the glass tube just before the bend and installing a silicone gasket that allowed smaller glass tubes with differing size sinus bulges to be inserted. Important for this set of experiments, these sinuses had ports for dye injection attached to the sinus bulges. Figure 2.3 shows the modified aortic arch model and different sinus bulge tubes. The pulsatile pump was set to a heart rate of 60 bpm

and a stroke volume of either 50 mL or 83 mL to match cardiac outputs of 3 liters per minute (lpm) or 5 lpm. These cardiac outputs were chosen because they encompass a low and average range for typical humans respectively.

In order to ensure that the conditions inside the aorta model were as close to philosophical typical as possible, the working fluid used for the Prosthetic Valve experiments was changed to a 50% water, 50% glycerol mixture. This mixture matches the viscosity of human blood when heated to body temperature. Over time, the water would evaporate and change the mixture's composition. To combat this, the mixture was weighed before every experiment to ensure that density was within 0.01 g/cm^3 of the target density to account for water evaporation[49].

Four different aortic replacement valves were tested. The valves tested were the 21 mm Tria valve, the 23 mm Tria valve, the 25 mm Tria valve and the 25 mm Perimount tissue valve. These valves were tested in several different configurations by changing the size of the sinus, or by mounting the valves with Cor-Knots.

We chose to use formation number as a metric to measure valve performance against. Formation number is a non-dimensional number that relates to the stroke ratio L/D of a column of liquid that enters a quiescent fluid bath as a jet. L is the length of the column and D is the diameter. The formation number has been studied extensively with respect to vortex ring formation. Gharib et al. (1998) showed that jets with a formation number less than 4 created single vortex rings. Jets with a formation number of more than 4 caused vortex rings to form in front of a trailing jet with secondary vortical structures. The leading vortex ring would always pinch off due to constraints on the amount of vorticity that the vortex ring could absorb before it pinched off from the trailing jets. More recently, researchers have applied formation number to the vortical structures seen in the heart in both *in vitro*[28] and *in vivo* studies[19]. We apply it to the flow in the aorta as a measure of the vorticity injected during each systole. The systolic formation number of each valve was found by calculating the stroke ratio L/D using the stroke volume of the pump and the Gross Orifice Area (GOA) of each valve. The GOA of a valve refers to the area of the orifice that a valve creates when it

is fully opened. The length L of the stroke ration was calculated by dividing the stroke volume of the pump by the GOA. D was calculated by assuming that the GOA was a perfect circle for each valve and solving for its diameter. The formation is calculated as follows:

$$\frac{L}{D} = \frac{V}{(\pi * (0.5\ d)^2) * d} \tag{1}$$

where V is the stroke volume, and d is the diameter of the valve.

Figure 2.3: Images of the two curved glass pipes that simulated the aortic arch. Top: Curved aorta with a 34 mm sinus bulge. Bottom: Curved glass aorta with interchangeable sinus bulge sizes (bottom right) Note that some sinuses had dye ports installed.

2.2 **Dye Measurements**

Fluorescent dyes were used as a measure of blood stasis and mixing around the valve in the following experiments. Dye was injected into the sinus through a port in the side of the bulge. The dye was comprised of 40% water, 60% glycerol, and 1 milligram per liter of fluorescent tracer dye (Bright Dyes Fluorescent Green Tracer 105001-1). The dye mixture was denser than the working fluid and would settle under the valve inside the sinus. The dye was illuminated by two UV handheld lights. These lights provided volumetric illumination of the sinus around the valve and of the dye as it moved throughout this volume. A microcontroller (Arduino uno) was retrofitted to the Harvard pump to synchronize the equipment to a specific phase of the cardiac cycle. A light detector measured the position of the piston inside the pump and a relay controlled whether the pump was on or off. After running the pump and ensuring that the water column was primed with liquid, the pump was stopped at the same point at the end of diastole to replicate the same settings for all experimental trials. Following pump setup, 1 mL of dye was injected into the sinus by a syringe pump. Once the experiment started, the microcontroller triggered a high-speed camera (Motionpro Y at 125 fps) to start acquisition as the pump was started. Each test run lasted ten seconds which allowed for 10 cardiac cycles to be recorded. Each dye test was repeated 3 times to ensure reproducibility. The dye concentration was carefully tuned to ensure that it would not saturate the camera sensor when it fluoresced from the UV illumination. Therefore the luminance values from the camera could be used to measure the concentration of dye over time throughout the sinus bulge.

All images were background subtracted by creating a maximum intensity projection of all frames from the last cardiac cycle of each data set. This maximum intensity projection created an image that was comprised of the brightest pixel values from the specified time period. The last cycle of the dye trials was used because all of the dye was washed away by this time so a background image of just the valve movement and reflections could be captured. This created a background image that ensured the motion of the valve would be removed from the fluorescence measurement and the dye fluorescence could be isolated.

Dye fluorescence measurements were computed by summing the pixel intensity of the area below the valve where the dye settled before the test. Only the pixels that originally contained dye were used in this sum. This provided a measure of dye washout over time after the cardiac cycle was started.

2.3 **DPIV Measurements**

Digital Particle Image Velocimetry (DPIV)[48] was utilized to measure the velocity field inside the model aortas. DPIV uses a high-speed camera to track the motion of particles as they are moved by the fluid motion. The fluid flows were seeded with silver-coated ceramic microparticles (20 micrometers in diameter) upstream of the valve. A continuous laser with a wavelength of 550 nm and 1 W power in combination with a cylindrical lens were used to illuminate the nanoparticles in a sheet that spanned the curve of the glass pipe. The laser sheet was positioned such that it would bisect mounted valve. An image depicting where the valve was illuminated can be seen in figure 2.5. Care was taken to ensure that the laser sheet was in the same location throughout all of the tests. A high-speed camera (Motionpro Y) was used to record the flow at either 500 or 600 frames per second. For the native valve experiments, the field of the view of the camera was positioned to record the flow entering the aorta through the heart valve and impingement areas of the systolic jet on the wall of the aortic arch. The Prosthetic Valve experiments used a smaller field of view focused on the sinus bulge to capture the velocity of fluid above and below the valve.

All images were preprocessed using a background subtraction algorithm where the average intensity was subtracted from the particle images. Qualitative streakline images were generated by applying the Kalman Stack filter in ImageJ[41]. This filter effectively superimposed the previous images of a sequence onto the analysis image. Each previous image was assigned a weight that decreased for images that were earlier in the image sequence. This produced an effect where particles would leave a streak with a tail that would become fainter. To further increase the visibility of the fluid's motion, ImageJ's Timelapse color coder tool was used to assign different colors to these superimposed images.

DPIV analysis was carried out using PIVview2C software. The inner and outer edges of the glass aorta and the valve were masked to be removed from quantification. Curves were fit to the mask points to mark the location of the boundaries for later analysis. The software provided time-varying velocity vector fields in the form of a Cartesian grid of discrete subsets, at the centroid of which each velocity vector is calculated.

2.4 **WSS Calculation**

The velocity vector fields measured by DPIV were used to calculate the velocity gradient values throughout the flow region, composed of the ascending aorta and aortic arch. The components (σ_{ij}) of the stress tensor were calculated using the following equation,

$$\sigma_{ij} = \mu\left(\frac{\partial u_i}{\partial x_j} + \frac{\partial u_j}{\partial x_i}\right) \tag{2}$$

where μ is the dynamic viscosity and $\frac{\partial u_i}{\partial x_j}$ and $\frac{\partial u_j}{\partial x_i}$ are components of the velocity gradients calculated from the PIV measurements. The stress tensor was then used to calculate the traction force vector ($\underline{t}$) on a curve S which is parallel and adjacent to the wall by using the Cauchy relation as follows:

$$\underline{t} = \underline{\underline{\sigma}} \cdot \underline{N} \tag{3}$$

where $\underline{N}$ is the wall unit normal vector. The traction vector was then decomposed along the wall unit tangent vector ($\underline{T}$) to calculate the shear stress (t_{wss}) at a given location as follows:

$$t_{wss} = \underline{t} \cdot \underline{T} \tag{4}$$

The wall-normal and tangent vectors were found using the same curves marking the wall boundaries used for the PIV analysis. To estimate the wall shear stress as accurately as possible, the aforementioned methodology was carried out as close to the wall as possible. The walls of the glass vessel were identified by hand and the velocity on the wall was clamped to zero. Data subsets that were directly adjacent to the inner and outer walls were

used to calculate the velocity gradients, and subsequently, the shear stress acting on the wall. The coordinate system used in this analysis is shown in figure 2.4.

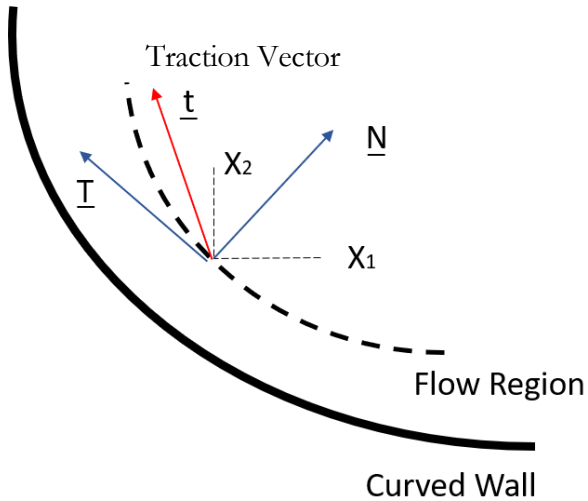

Figure 2.4: Coordinate System used for WSS measurements

2.5 **Residence Time Calculations**

During the native valve experiments, residence time analysis was carried out using a simulated particle tracking algorithm. Simulated particles were seeded inside the flow field. The subsequent position of each particle was then estimated for each time step using the velocity field data from the PIV analysis. This analysis was carried out throughout a whole cardiac cycle starting at peak diastole. An area of interest near the top leaflet was designated as shown in Figure 2.5. The number of particles that started inside and ended inside the area during one cardiac cycle was then measured to produce a metric for how long blood remains stationary near the leaflet. The top leaflet was chosen because it was the only leaflet which was bisected by the laser sheet used for PIV measurements. On the bottom portion of the heart valve, the laser sheet bisected the post that supports the bottom two leaflets, so the residence time was ignored in this region.

Residence time was estimated for the replacement/prosthetic valve experiments by calculating the average and the standard deviation of the velocity at specific points around

the different valves. These metrics will be referred to as mixing metrics when discussing their effects on the blood and valves. Average velocity serves as a measure of blood washout while velocity standard deviation relates to the turbulence intensity of the blood in the region[17]. Simulated particle tracking was not used for these experiments because the differing sinus and valve sizes made it unmanageable to ensure that each experimental configuration had an adequate number of simulated particles and velocity information. Furthermore, small gaps between the valve and the wall made it very likely that simulated particles would collide with the wall and remain stuck at the no slip boundary condition set there. These particles would interfere with the counting algorithm and degrade the quality of the measurement in these areas.

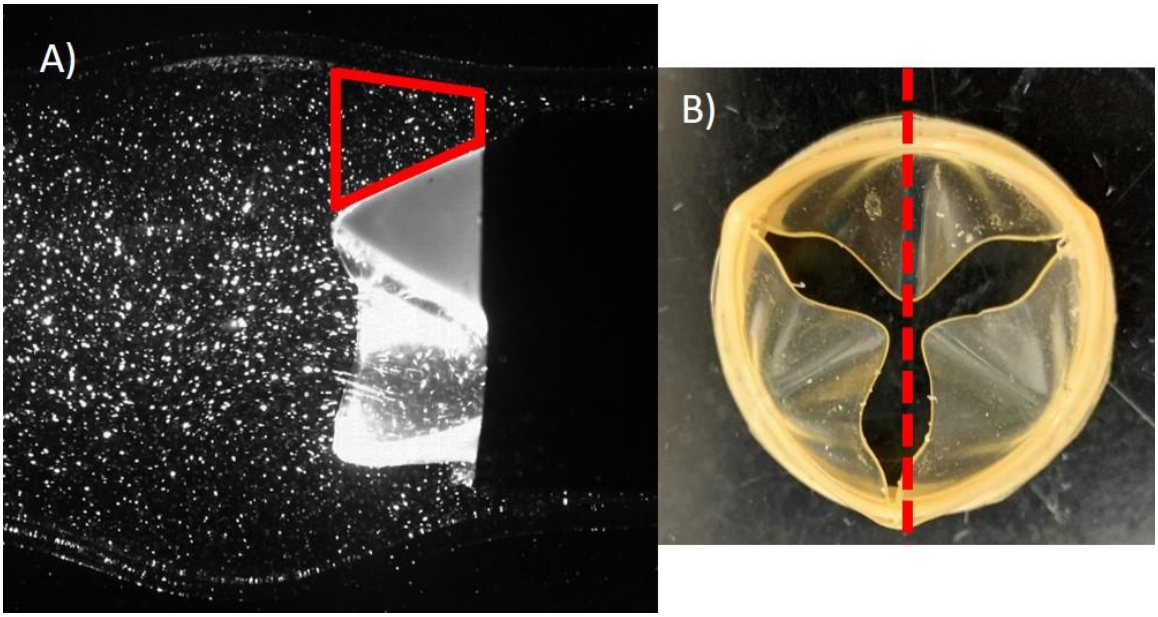

Figure 2.5: : A) The red box indicates the area that was used to calculate the residence time. Particles that started and ended this area were counted as having remained. B) A depiction of where the laser sheet intersected the heart valve. Only the top leaflet was illuminated enough for data acquisition.

Chapter 3

Results

This chapter is dedicated to presenting our results on the hemodynamics caused by aortic valves inside our aorta model.

3.1 **Native aortic valve and leaflet stiffness asymmetry**

3.1.1 **Qualitative Flow Measurements:**

To better understand how different valve leaflet stiffnesses affect the downstream distribution of wall shear stress, we first examined general flow patterns created by the valves inside the ascending aorta. Figure 3.1 depicts the streak visualization of the flow during peak systole for all four configurations. The baseline (ST) valve shows the flow features that would typically be present during systole, a wide central jet that expands out and slows down as it enters the aortic arch. Small recirculation regions were present above and below the systolic jet inside the sinus bulge. The stenotic valve (SS) also exhibits a distinctive systolic jet that travels along the center of the ascending aorta. However, the jet has a higher velocity because of its decreased effective orifice area when compared to the typical case. This leads to a narrower jet and creates larger recirculation regions near the walls. The configuration with a single stiffened leaflet near the inner wall (A1) deflects the systolic jet towards the outer wall of the ascending aorta. It creates a large recirculation region near the inner wall. The jet impinges directly into the outer wall of the ascending aorta. This flow pattern closely matches the flow created by a Björk-Shiley tilting-disc valve, which in some cases, was thought to contribute to the formation of saccular aneurysms in patients[36,42]. Finally, the valve with two stiffened leaflets near the outer wall (A2) deflects the systolic jet towards the inner wall and creates the recirculation region near the outer wall. The systolic jet in this configuration more closely followed the anatomical curve of the aorta, which delayed jet wall impingement. For completeness, the time series of the evolution for each configuration's systolic jets and the recirculation regions is presented in Appendix A. These time-lapses

provide detailed context for the observations discussed above in relation to the comparisons shown in Figure 3.1.

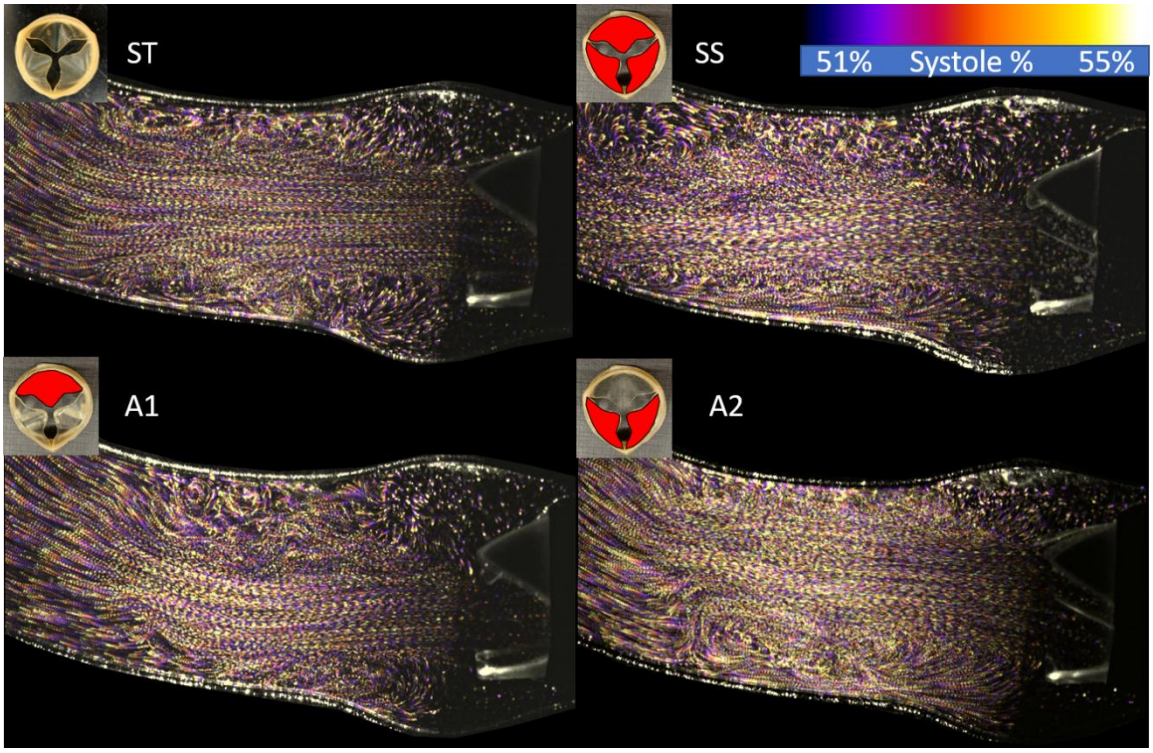

Figure 3.1: Streak Images for each configuration. Each image was composed of a superposition of the 10 images that spanned 51% of systole to 55% (which equates to 46 milliseconds, 509 milliseconds after systole began) of systole when the velocity of the fluid was highest.

3.1.2 **Systolic Jet Velocity Profile:**

To quantitatively measure the effects of leaflet asymmetry, the velocity profile of the fluid 20 mm downstream of the valve was analyzed. These measurements serve as the entry condition for the flow into the aorta. The velocity profile of the fluid during peak systole for each experimental configuration is presented in Figure 3.2. As would be expected, the ST configuration of the valve produces a fairly uniform velocity profile with a peak velocity of 0.85 m/s. The stenotic, SS, configuration produces a symmetric profile with a peak velocity of 1.7 m/s. This occurs because the stiffer leaflets do not open fully, decreasing the effective

orifice area of the valve. Given that the pulsatile Harvard pump was set to the same stroke volume for all configurations, the same volume of fluid had to be pumped through a smaller area, dramatically increasing the peak velocity during systole. This configuration also exhibits a large degree of reverse flow back towards the valve around the sinus bulge. Both the single stiffened leaflet (A1) and the double stiffened (A2) configuration produced asymmetric velocity profiles where higher velocity fluid was diverted away from the stiffened leaflets. Furthermore, the number of stiffened leaflets affected the effective orifice area of the valves and their respective peak velocities. In the A1 configuration, the systolic jet was vectored directly into the outer wall, whereas the A2 configuration vectored the jet towards the inner arch wall.

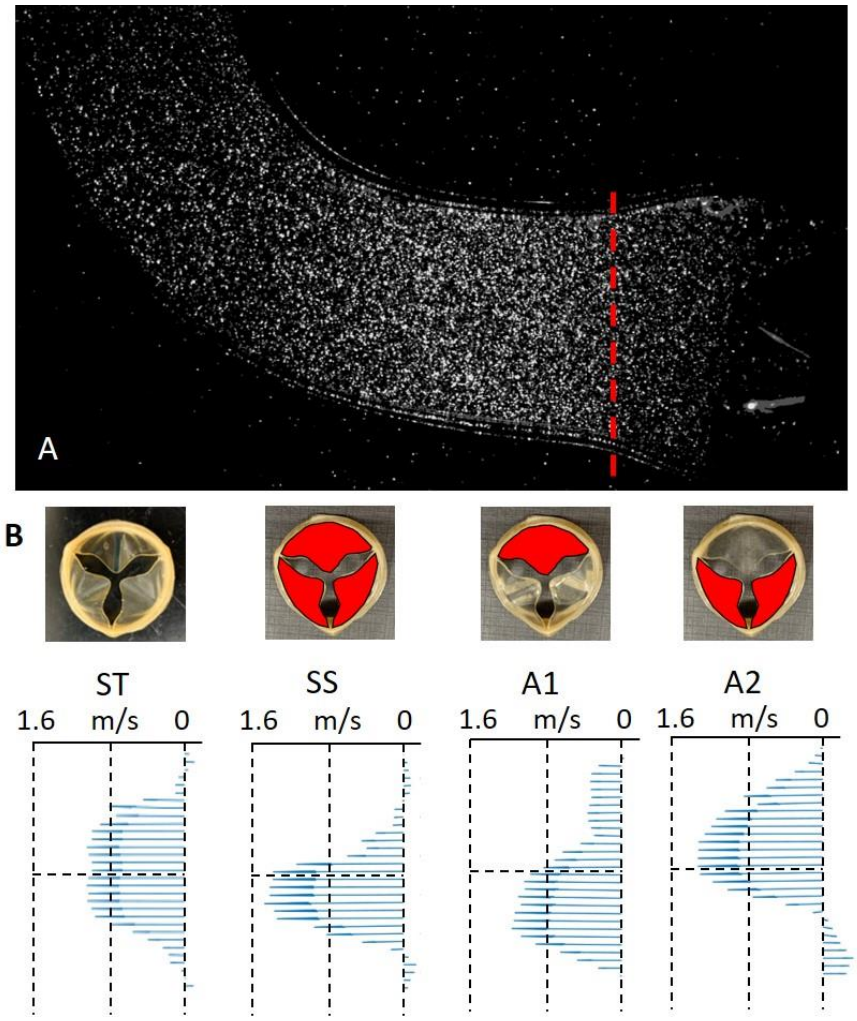

Figure 3.2: **A:** Image captured from the high-speed camera showing a typical particle image. The red dotted line indicated the location from which the velocity profile data in B was taken. **B:** Velocity vector data plots for the four different experimental configurations during peak systole.

3.1.3 **Wall Shear Stress**

Wall shear stress is directly related to the velocity gradient of the fluid flow in the vicinity of the wall. Therefore, it would be expected that the valve configuration that produces a systolic jet with the highest velocity would produce the largest wall shear stress where the jet impinges on the wall. However, Figure 3.3 shows how the stiffness (resulting in angled jet trajectory) of the valve plays a much larger role in the distribution of wall shear stress. Both

of the symmetric configurations (ST and SS) follow the same spatial distribution along the inner and outer walls, where the only major difference is that the stenotic SS case has a larger overall magnitude. The A1 configuration has the largest overall average wall shear stress, even though it has a lower peak velocity than both the A2 and SS configurations. This is because the single stiffened leaflet near the inner wall of the aortic arch directs the systolic jet towards the outer wall of the arch, which leads to very early wall impingement. The A2 configuration produces the second lowest wall shear stress because it deflects the systolic jet along the direction that the aortic arch is bending. Therefore, the jet has more time to disperse its kinetic energy into the surrounding fluid before it reaches the wall. Furthermore, the A2 configuration reduces the average wall shear stress on the inner wall of the arch, which may be caused by a decrease in the amount of reverse flow near the inner wall.

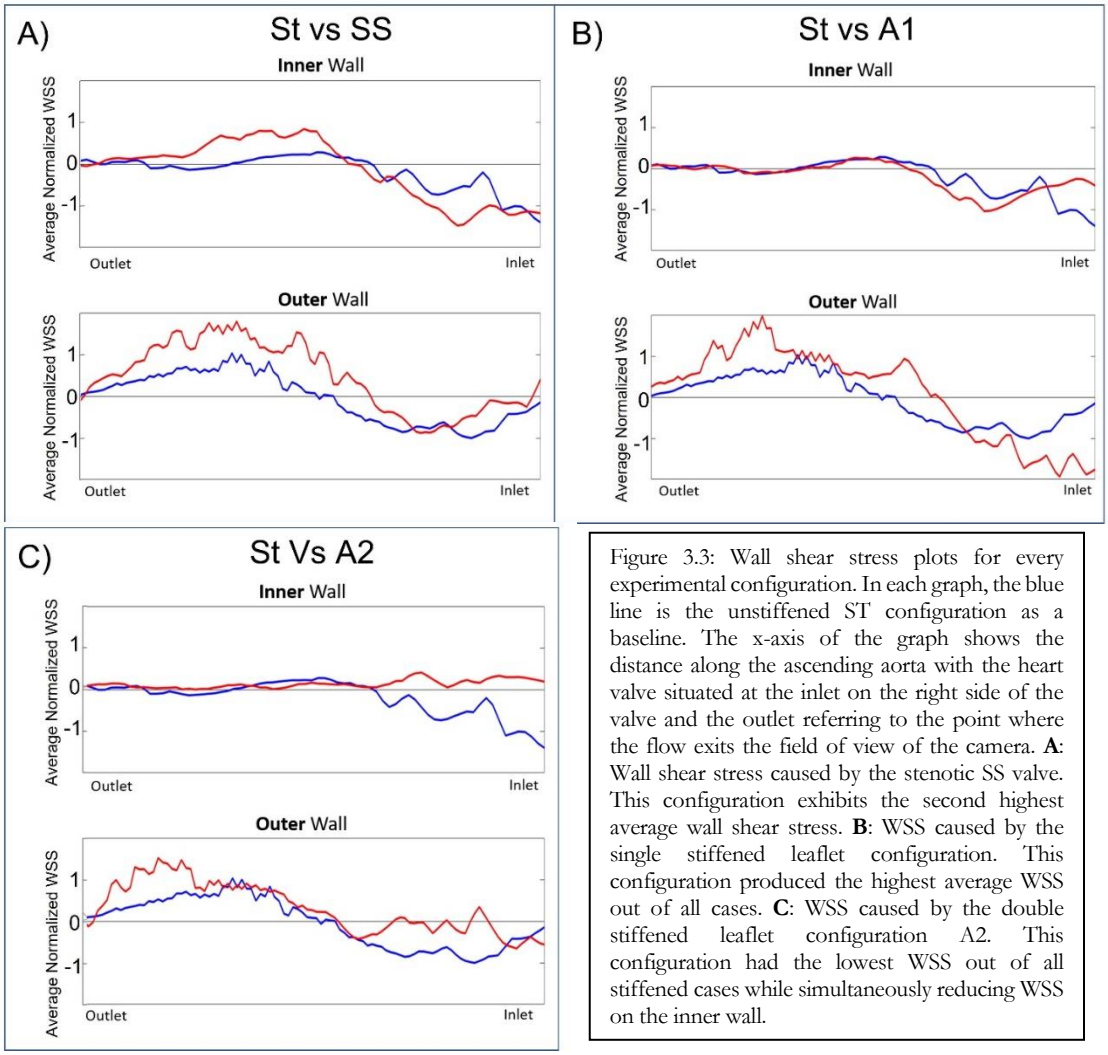

Figure 3.3: Wall shear stress plots for every experimental configuration. In each graph, the blue line is the unstiffened ST configuration as a baseline. The x-axis of the graph shows the distance along the ascending aorta with the heart valve situated at the inlet on the right side of the valve and the outlet referring to the point where the flow exits the field of view of the camera. **A**: Wall shear stress caused by the stenotic SS valve. This configuration exhibits the second highest average wall shear stress. **B**: WSS caused by the single stiffened leaflet configuration. This configuration produced the highest average WSS out of all cases. **C**: WSS caused by the double stiffened leaflet configuration A2. This configuration had the lowest WSS out of all stiffened cases while simultaneously reducing WSS on the inner wall.

3.1.4 **Residence time**

Figure 3.4 shows the fraction of simulated particles that remained near the topmost leaflet during a single cardiac cycle. The highest residence times are associated with the SS and A1 configurations. Both configurations had a stiffened upper leaflet, which indicates that stiffening a leaflet leads to less reverse flow in the sinus directly behind the stiff leaflet. The A2 configuration exhibited the lowest residence time ratio which is most likely attributed to how this configuration vectored the systolic jet upwards towards the inner wall and increased the profusion near the unstiffened leaflet. Furthermore, the unstiffened leaflets could move freely, which prevents blood flow from remaining stagnant in the sinus behind these leaflets.

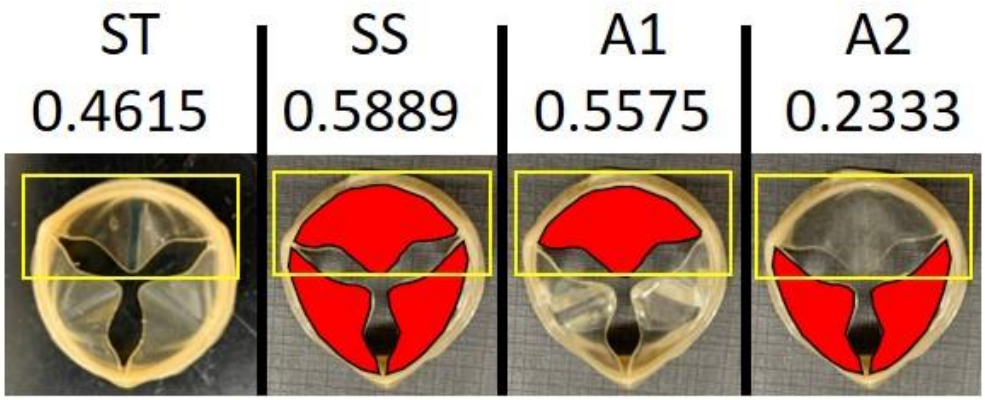

Figure 3.4: The ratios of the particles that started and ended near the top leaflet (boxed in yellow). Stiffened upper leaflets had a higher residence time ratio.

3.2 **Prosthetic Valve Hemodynamics**

3.2.1 **Prosthetic Valve Sizing**

Valve and sinus sizing were investigated to determine their effect on blood stasis and residence time

3.2.1.1 **Dye Visualization**

Dye visualization was used as a tool to measure the performance of different valves and sinus combinations. Figure 3.5 shows a time sequence of the 23 mm Tria valve and the 25 mm Tria valve in a 32 mm sinus. It is immediately apparent that the 25 mm Tria valve clears less of the dye after each subsequent cycle. Moreover, the 23 mm Tria valve is able to completely remove the dye from the outer wall after one cycle whereas the 25 mm Tria has dye adhering to the sinus wall for several cycles. Figure 3.6 presents the quantitative fluorescence measurements for the area under the valve for the three Tria valve sizes tested (21 mm, 23mm, and 25 mm). The 21 mm valve and the 23 mm valve both clear the majority of the dye in a single cardiac cycle. The 25 mm, as described previously, lags by several cycles in

both the low flow rate of 3 lpm and the high flow rate of 5 lpm. Figure 3.7 compares the 23 mm Tria Valve with the 25 mm Perimount tissue valve. The gross orifice area (GOA) of these valves is similar, however the tissue valve is bulkier than the Tria valve. Overall, the tissue valve exhibits a similar amount of dye residence to the 23 mm Tria valve. However, the bioprosthetic valve clears the dye later than the 21 mm and 23 mm polymer valves. The polymer valves seem to start clearing during systole whereas the Perimount valve clears dye during diastole. The 23mm Tria valve was then tested in sinuses of different sizes. Figure 3.8 summarizes the comparison between the 29 mm, 32 mm, and 33.5 mm sinuses. Generally, each configuration cleared most of the dye in a single cardiac cycle with very little variation.

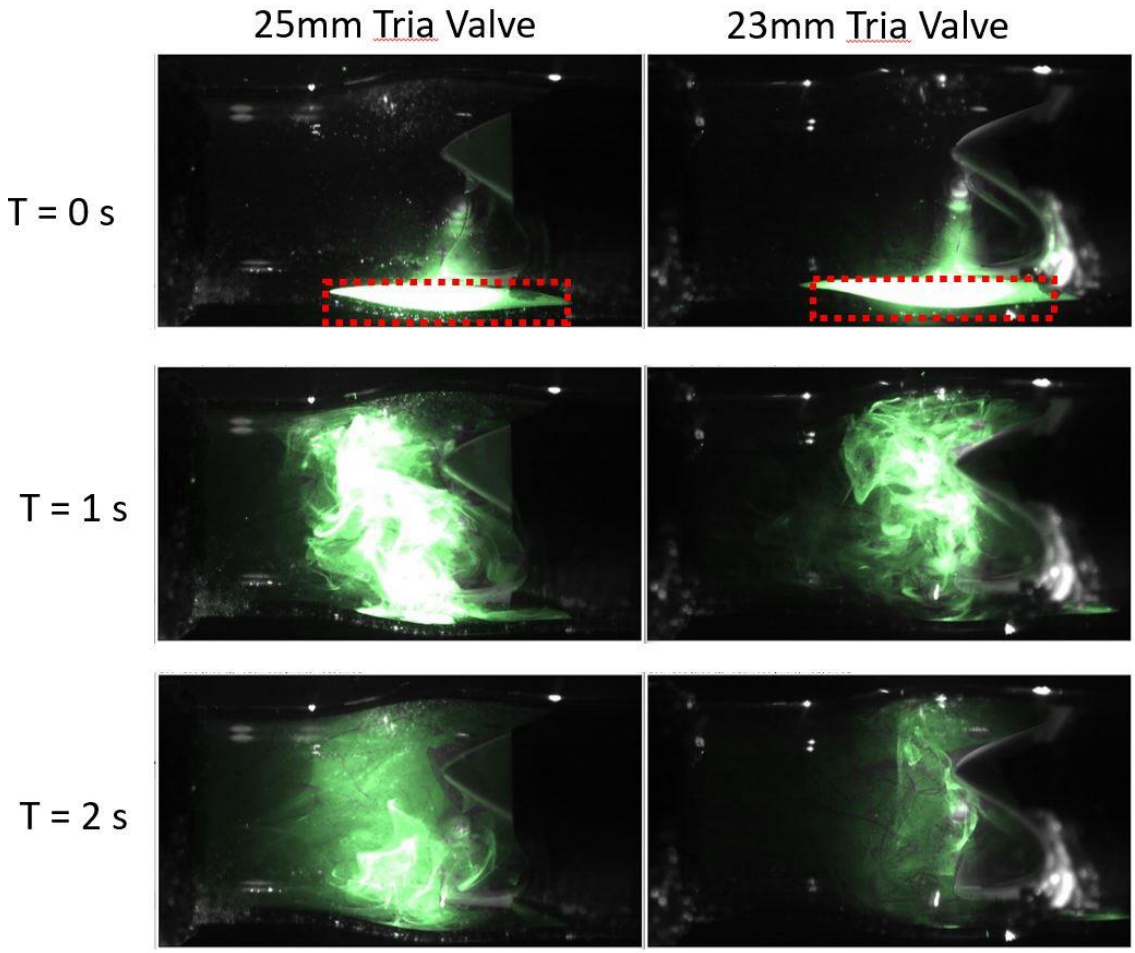

Figure 3.5: Time sequence of color enhanced dye images. At t = 0 the pump has not been activated and the negatively buoyant dye has

settled underneath the valves inside the sinus. At t = 1 second, one cardiac cycle has passed. Note how more dye remains on the wall with the 25 mm Tria valve experiment than the 23 mm Tria valve. At t = 2 seconds, a second cardiac cycle has occurred and the 25 mm Tria has cleared less dye than the 23 mm Tria valve. The red boxes denote where the dye fluorescence quantification occurs in the subsequent plots.

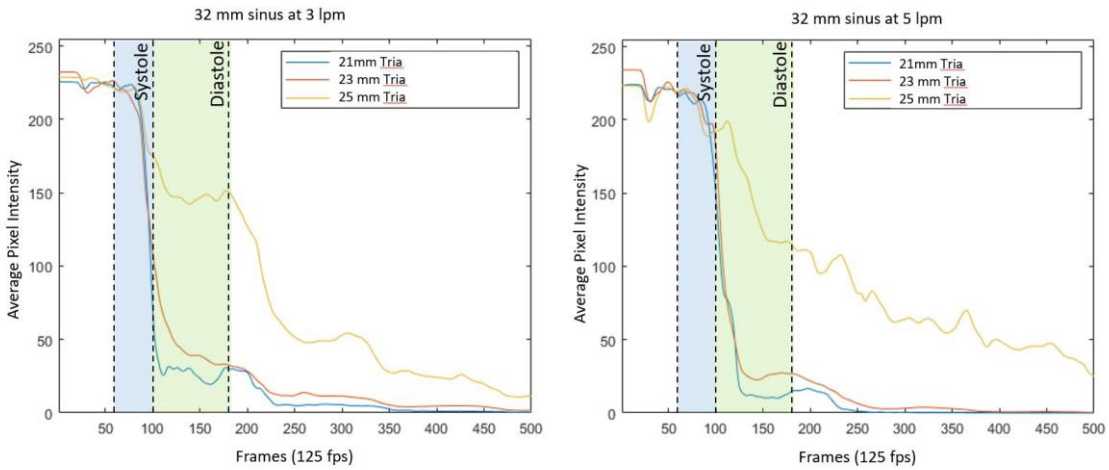

Figure 3.6: Dye Fluorescence quantification in the area between the post and the sinus wall. In this experiment, sinus bulge diameter was held constant and different size polymer valves were tested over several cycles. The blue bar denotes when the first systole occurred, and the green bar denotes when the first diastole occurred.

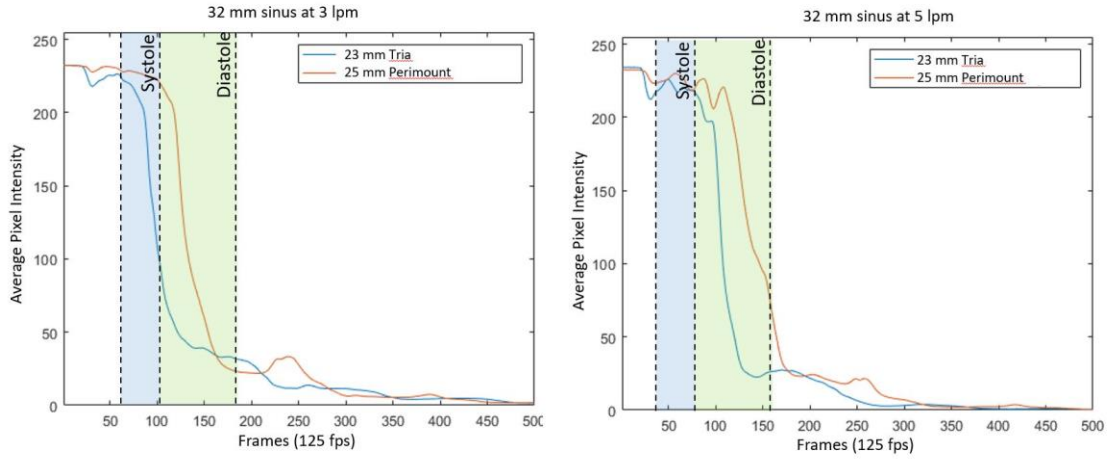

Figure 3.7: Dye Fluorescence Quantification of a 23 mm Tria valve and a 25 mm Perimount valve inside a 32 mm sinus bulge.

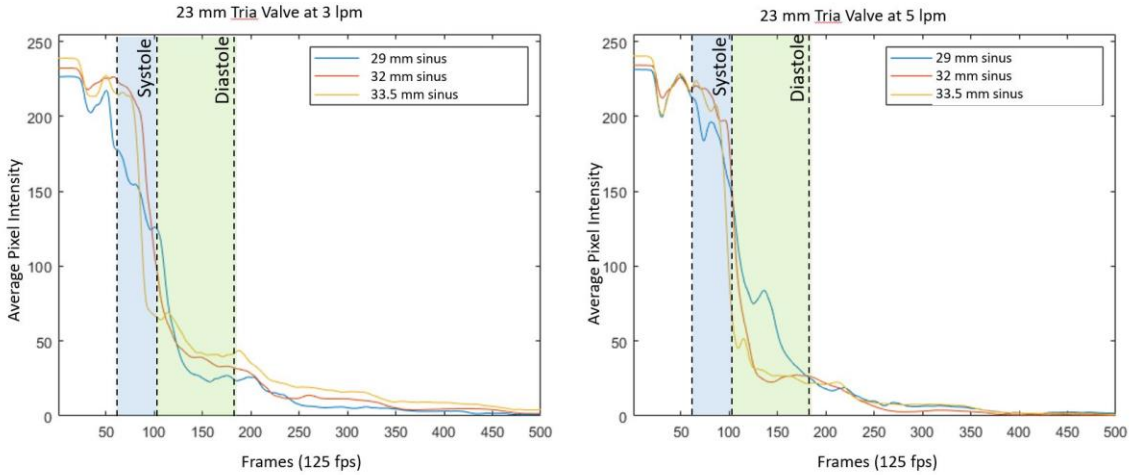

Figure 3.8: Dye Fluorescence Quantification of a 23 mm Tria valve inside a 29 mm, 32 mm sinus, and a 33.5 mm sinus.

3.2.1.2 **PIV Velocity Measurements**

Quantitative velocity information from around the valve was then measured using PIV. Figure 3.9 shows the average velocity color contour map around the valves computed over 4 cycles. This data serves to illustrate that having oversized valves inside of narrow sinus bulges tends to create regions of low average flow velocity and standard deviation, indicating low levels of mixing and increased blood residence time.

Next, individual points near the leaflets were analyzed to better understand the hemodynamics in that region. These points were selected by finding the midpoint between the valve and the wall both above the leaflet and below the post. Figure 3.10 presents both the average velocity and the velocity standard deviation plotted against the formation number of the valve during systole. The formation number can be understood as a measure of vorticity injected into the aorta and is impacted by the valve GOA and the cardiac output of the heart. Smaller valve GOAs and larger cardiac outputs would lead to larger formation numbers. In the areas near the leaflets, the average velocity, standard deviation, and therefore fluid washout increase linearly with increasing formation number.

However, the area between the valve post and the sinus wall did not follow the same trend as the space near the leaflets. Figure 3.11 shows how the average velocity and velocity standard deviation does not necessarily increase with increasing formation number. Instead, the dominant parameter in this area is the physical distance of the gap between the post and sinus wall as seen in figure 3.12.

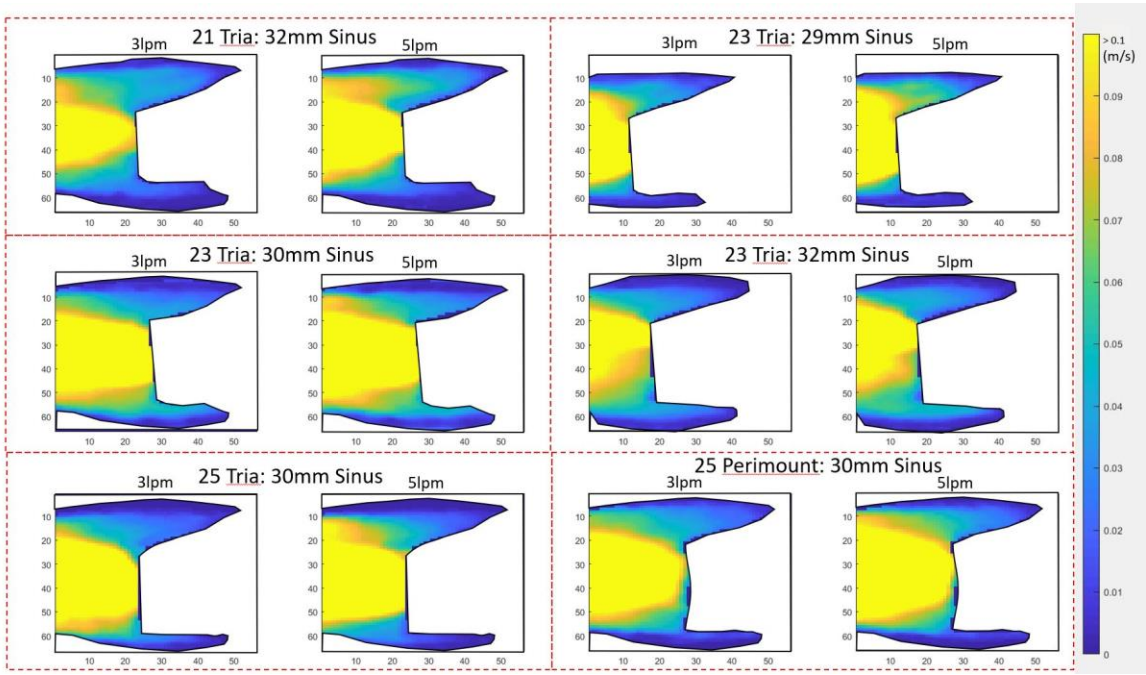

Figure 3.9: Average velocity heatmap for several different test configurations. Note how smaller sinuses tended to create slower average flow velocities between the post and the sinus wall.

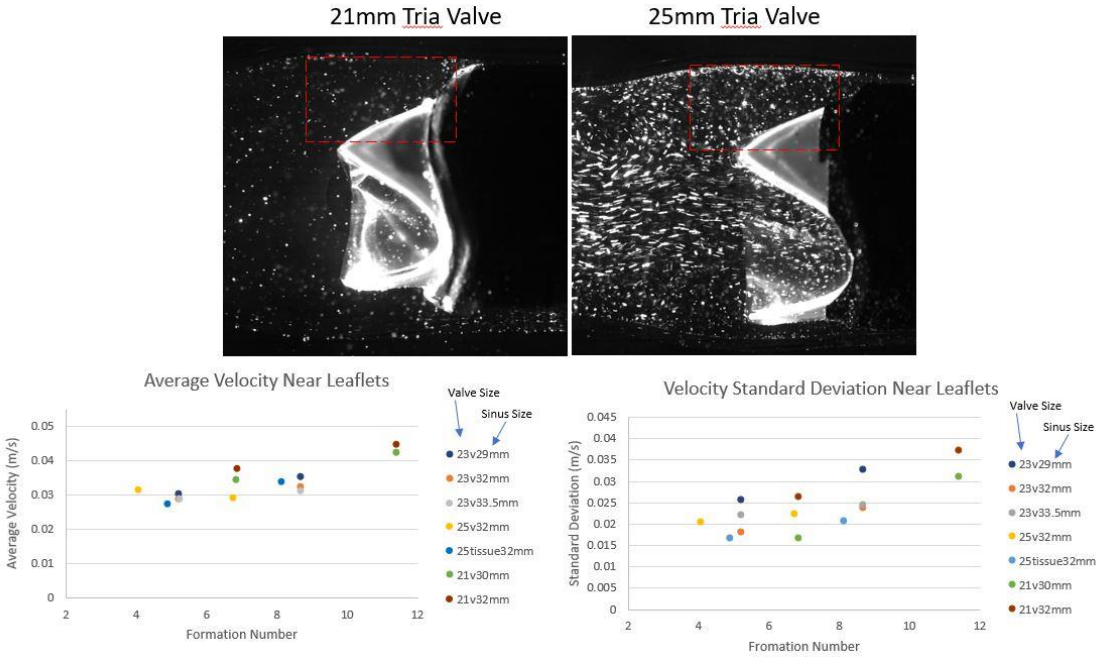

Figure 3.10: Mixing metrics are plotted against systolic formation number. The mixing metrics were measured in the area above the valve leaflets and are denoted by the red dashed lines in the images above. In the legend, v stands for Tria valve and tissue refers to the Perimount valve.

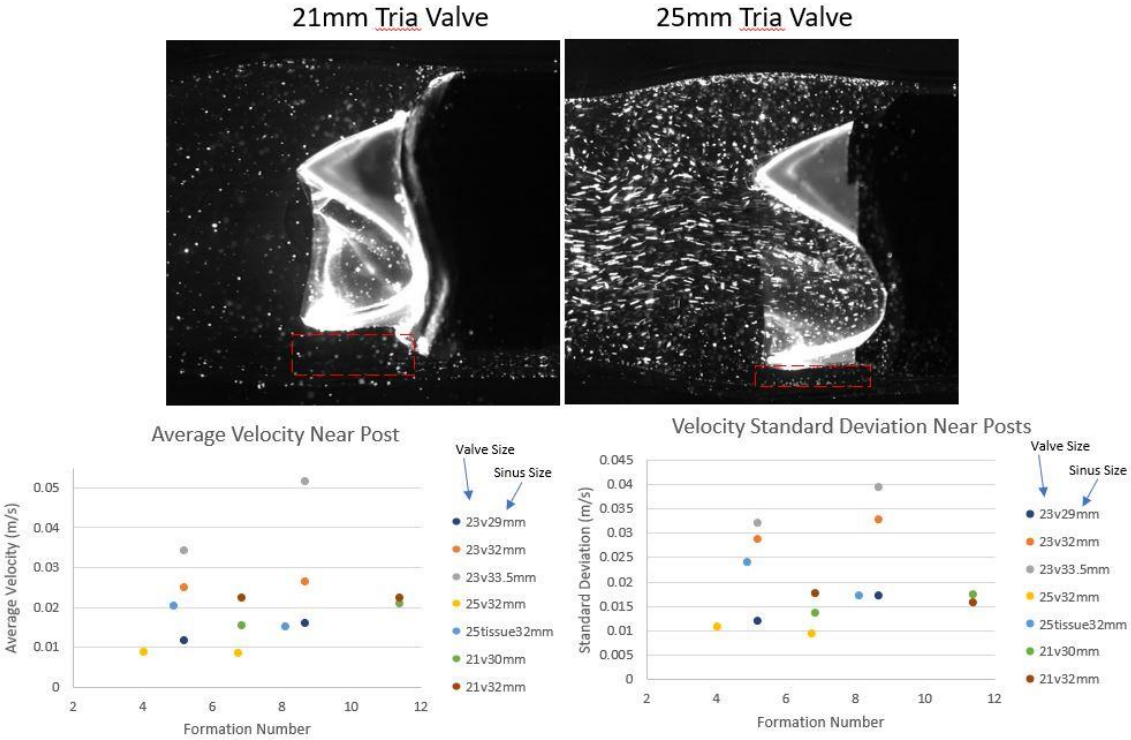

Figure 3.11: Mixing metrics are plotted against systolic formation number. The mixing metrics were measured in the area between the valve posts and sinus wall and are denoted by the red dashed lines in the images above. In the legend, v stands for tria valve and tissue refers to the Perimount valve.

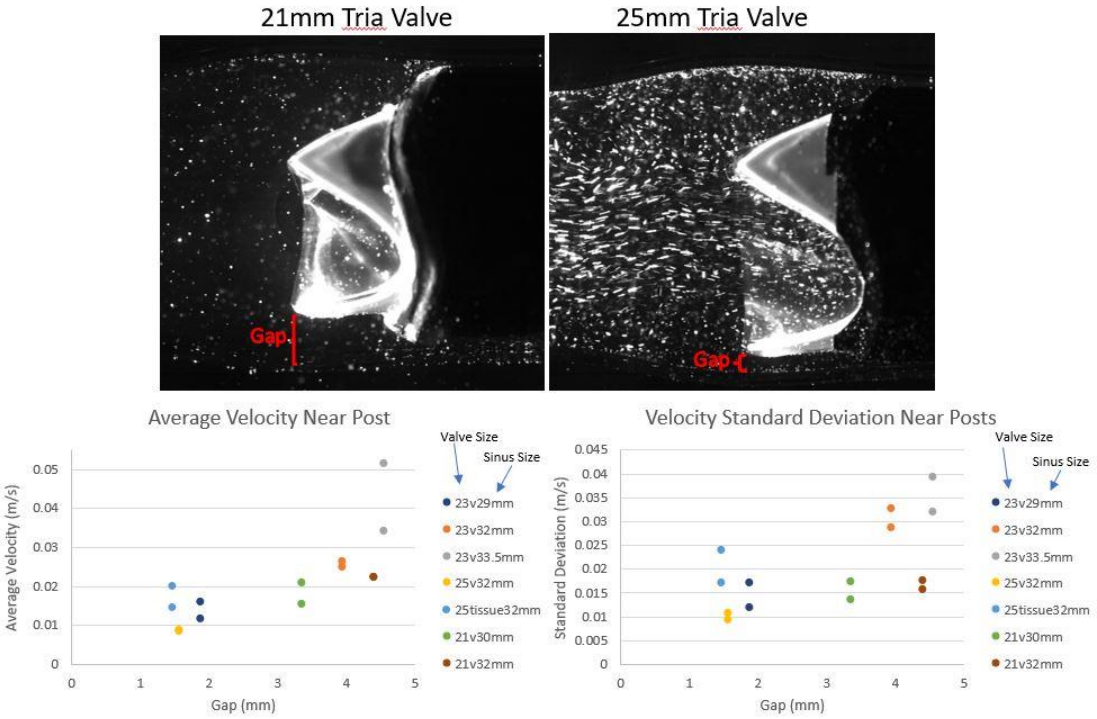

Figure 3.12: Mixing metrics are plotted against the distance between the valve post and the sinus wall (gap distance). In the legend, v stands for tria valve and tissue refers to the Perimount valve.

3.2.2 **Valve Mounting Geometry**

The effect of mounting the valves with Cor-Knots was studied.

3.2.2.1 **Dye Visualization**

Dye experiments provided a measurement of the impact of Cor-Knots on the blood flow surrounding the valves. Figure 3.13 shows an example time series comparing the 25 mm Perimount tissue valve with and without Cor-knots. The injected dye stays adhered to the outer sinus wall for over two cardiac cycles when Cor-knots are present whereas the normally mounted valve clears most of the dye from the wall after a single cycle. Figure 3.14 shows the decay of fluorescence in the area where the dye settled before the heart pump was

activated. As opposed to the oversized valves who failed to clear dye within a single cycle regardless of cardiac output, increasing cardiac output when Cor-knots are present improves the washout of the valves. This is also observed with the 23mm Tria valve in figure 3.15. At 3 lpm, the 23mm Tria valve mounted with Cor-Knots performs much worse than the same valve without Cor-Knots. However, when the valve size in decreased to 21 mm, dye is efficiently cleared regardless of the presence of Cor-Knots and cardiac output (figure 3.16).

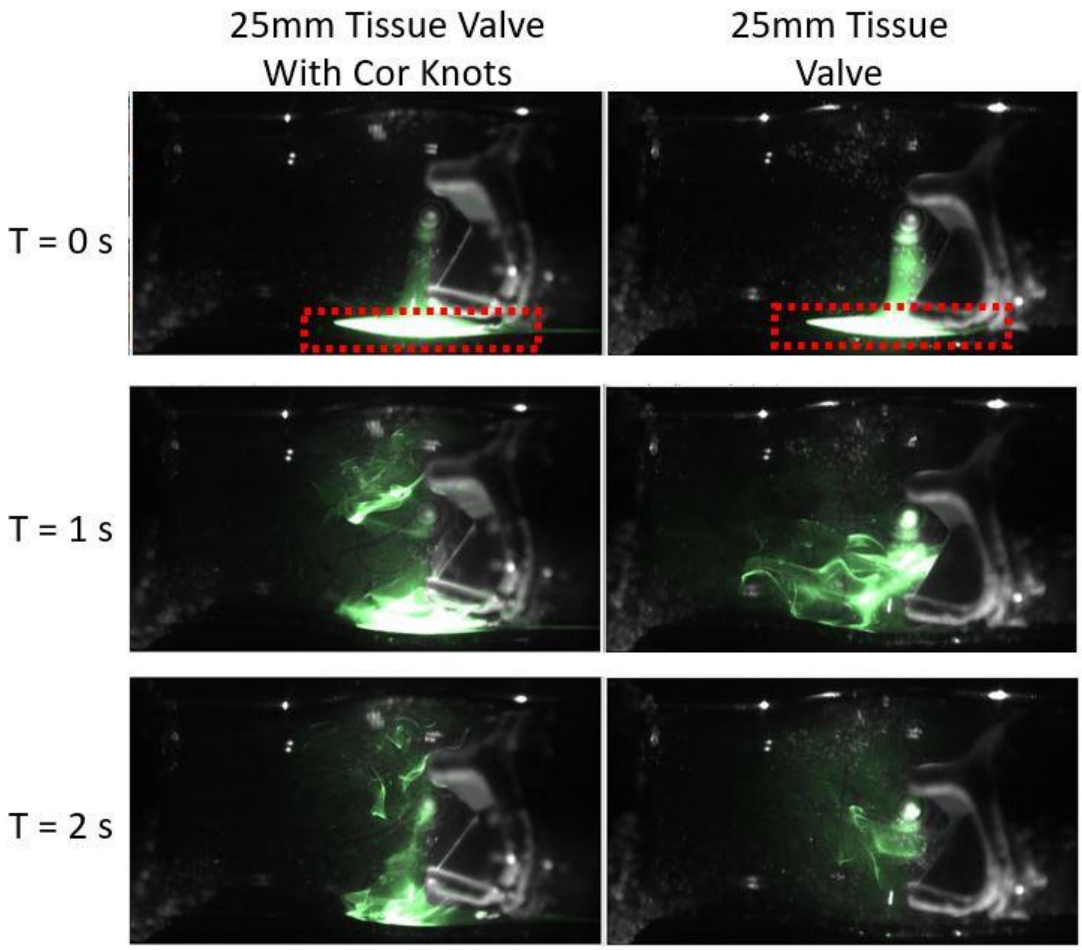

Figure 3.13: Time sequence of color enhanced dye images. At t = 0 the pump has not been activated and the negatively buoyant dye has settled underneath the valves inside the sinus. At t = 1 second, one cardiac cycle has passed. Note how more dye remains on the wall with the Cor-Knot valve experiment than the 25 mm Tissue valve. At t = 2 seconds, a second cardiac cycle has occurred, and the 25 mm Tissue with Cor-knots has cleared less dye than the 25 mm Tissue valve. The red boxes denote where the dye fluorescence quantification occurs in the subsequent plots.

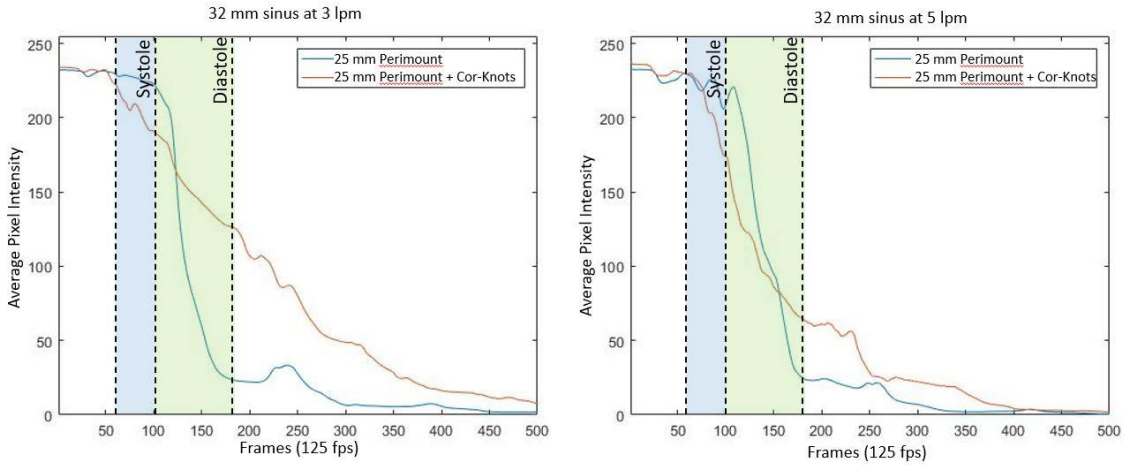

Figure 3.14: Dye Fluorescence quantification in the area between the post and the sinus wall. Both tests used the same sinus and 25 mm Paramount valve. However, during one of the tests, the valve was mounted with Cor-knots. The blue bar denotes when the first systole occurred, and the green bar denotes when the first diastole occurred.

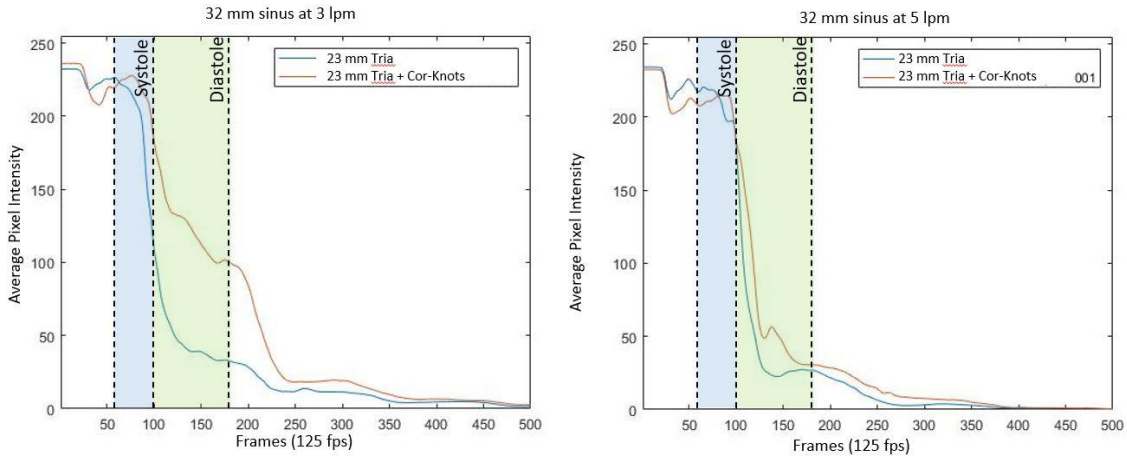

Figure 3.15: Dye Fluorescence quantification of the Cor-knot equipped 23mm Tria valve versus the 23mm Tria without Cor-knots The blue bar denotes when the first systole occurred, and the green bar denotes when the first diastole occurred.

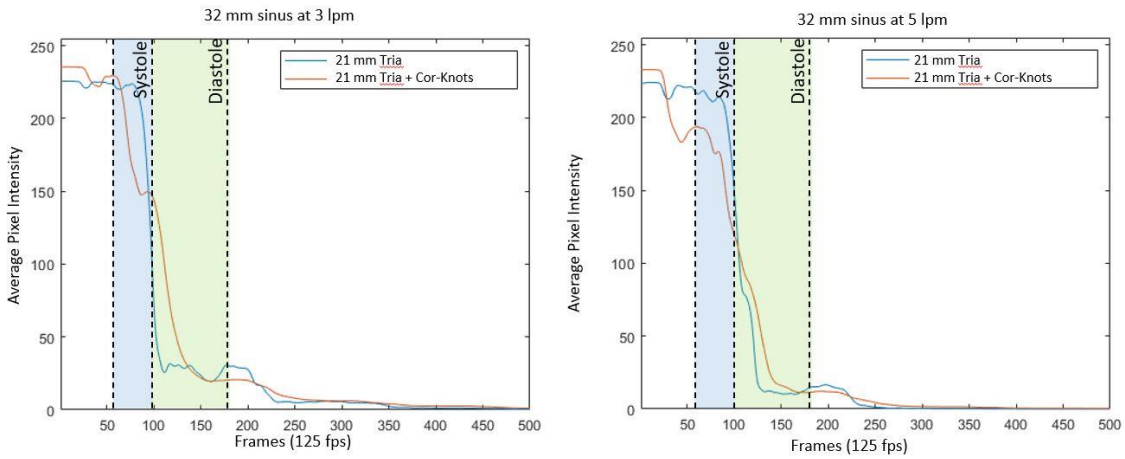

Figure 3.16: : Dye Fluorescence quantification of the Cor-knot equipped 21mm Tria valve versus the 21mm Tria without Cor-knots The blue bar denotes when the first systole occurred, and the green bar denotes when the first diastole occurred.

3.2.2.2 **PIV Velocity Measurements**

PIV provided time-varying velocity information around the different valves which was used to measure the effective mixing and fluid stasis around the Cor-knots at the base of the valve. The area above the leaflets was analyzed first. Figure 3.17 compares the average velocity and velocity standard deviation of valves with and without Cor-Knots by plotting them against the Formation Number. In every case, the valves equipped with Cor-Knots underperform and fall below the trend of the valves without Cor-knots. The 21 mm Tria valve is least affected by the presence of Cor-knots which is consistent with the dye studies performed in the previous section.

The area between the valve posts and the sinus wall was analyzed next. Figure 3.18 presents the average and standard deviation of the velocity plotted against the gap distance (the distance between the post and the sinus). This region follows a similar trend as the region near the valve leaflets with Cor-Knots valves performing slightly worse in both average velocity and standard deviation. This occurs despite the Cor-Knot valves having a slightly larger gap distance. This gap increase is most likely caused by the Cor-Knots themselves causing the valves to be slightly shifted upwards.

Finally, figure 3.19 shows the average velocity fields of the 23mm Tria valve with and without Cor-Knots. The presence of the individual Cor-knots dampens the average velocity in their vicinity at low cardiac outputs. However, increasing the cardiac output did serve to reduce the effect that the Cor-Knots had on the surrounding flow.

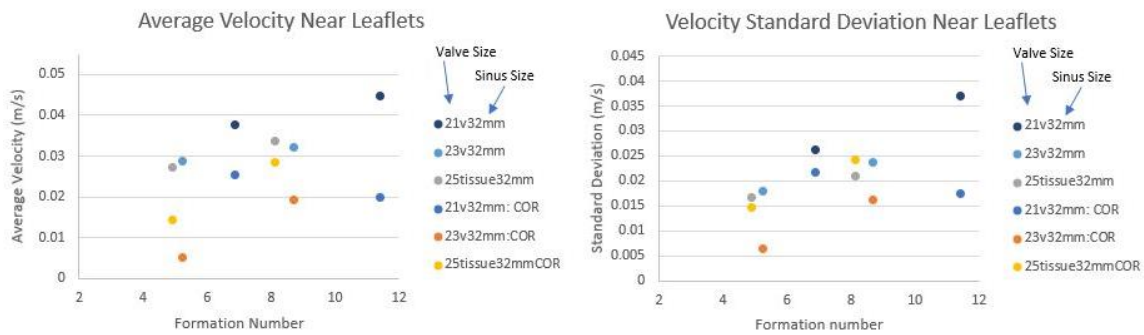

Figure 3.17: Mixing metrics for valves with and without Cor-knots plotted against formation number. In the legend, v stands for tria valve and tissue refers to the Perimount valve.

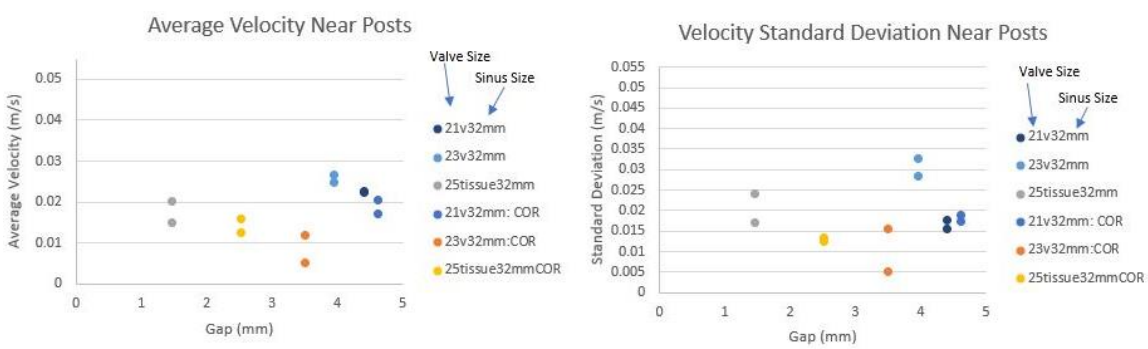

Figure 3.18: Mixing metrics for valves with and without Cor-knots plotted against gap distance. In the legend, v stands for tria valve and tissue refers to the Perimount valve.

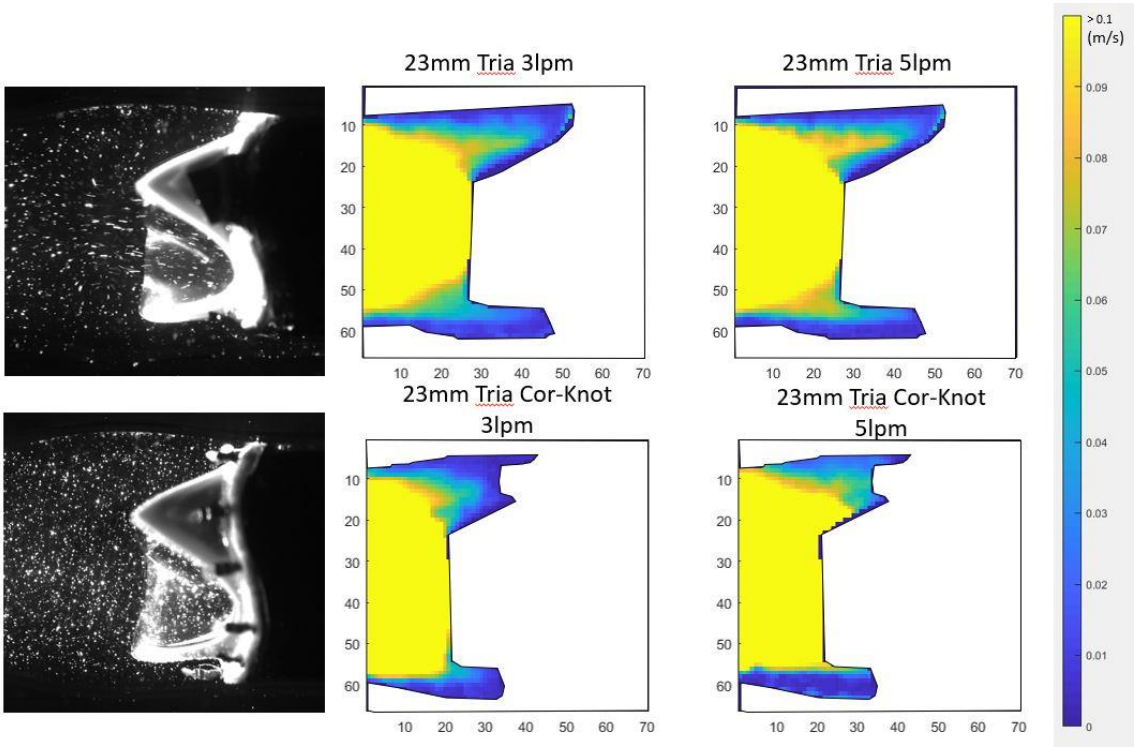

Figure 3.19: Average Velocity Heatmaps of the 23 mm Tria valve with and without Cor-Knots.

Chapter 4

Discussion

4.1 **Native aortic valve and leaflet asymmetry**

The stiffness of the individual leaflets, and hence the opening geometry of the tri-leaflet aortic valve, heavily influences the downstream hemodynamics in the ascending aorta. The first, most apparent effect is the gradual decrease in the effective orifice area of the valve as leaflets are stiffened. This leads to higher systolic jet velocities and increased WSS from systolic jet impingement on the wall. These findings were to be expected and match closely with results from previous studies[25,30,37,38]. However, Oojj et al. (2017) remarked that different AS patients had highly variable flows and that AS was the dominant factor when compared to other factors such as bicuspid aortic valves[38]. This work was an expansive study that averaged results over hundreds of patients. However, by averaging their results, they could not draw specific conclusions from individual patient's stenotic valvular geometries. This illustrates the impact stenosis, and more importantly, the non-uniform stiffening of aortic leaflets can have on the hemodynamics in the aorta. Our systemic approach allowed us to illuminate the complex effects that non-uniform leaflet stiffening create in the aorta. When only one or two leaflets are stiffened, the systolic jet is vectored away from the stiffened leaflets. In effect, the eccentricity of the systolic jet is increased in a predictable fashion with the jet being diverted away from the stiffened leaflets. The eccentricity of the systolic jet directly influences the distribution of WSS, with the highest WSS being located where the jet impinged on the aortic wall. Notably, the valve configuration that produced the highest WSS was the A1 valve, even though this valve had second largest effective orifice area and the second lowest systolic jet velocity. In a clinical setting, an analogous valve with a single stiffened leaflet would be classified as less stenotic than the A2 and SS valve configurations because it would perform better in all ACC/AHA guideline metrics[3]. However, the high WSS exhibited by the A1 configuration could lead to conditions similar to those created by bicuspid valves and mechanical valves where highly eccentric systolic

jets were thought to cause the growth of saccular aneurisms in the ascending aorta[31,36,42]. The A2 configuration produced the lowest WSS of any stiffened leaflet configuration even though it exhibited a higher jet velocity and a smaller valve area. This illustrates how the WSS distribution in an aorta is highly dependent on the individual stiffnesses of the upstream valve. The leaflet stiffening also heavily influenced the residence time of the fluid directly adjacent to the valves. Stiffer leaflets consistently increased the number simulated particles that remained near the leaflet over one cardiac cycle. This is likely due to the fact that the stiffened leaflets could not open properly, and the eccentricity of the systolic jet caused there to be low flow velocities behind the stiffer leaflets. This would theoretically lead to a higher chance of thrombus in the sinus bulge.

The aforementioned work on Aortic Stenosis serves two purposes. Firstly, it models and visualizes the hemodynamics associated with the disease states found in aortic stenosis so that they can be better understood and accurately simulated. The data presented above can be used to validate detailed numerical simulations of the aforementioned disease. Secondly, it shows how WSS can be controlled through careful manipulation of the aortic valve's individual leaflet thicknesses. A creative potential application of this work is the downstream control of the systolic jet through the customization of valve leaflet stiffnesses, which could be used to tailor replacement prosthetic heart valves to individual patients. However, care must be taken to balance the amount of leaflet stiffening with the decrease in the effective orifice area and the increase in the residence time inside the sinus. While the level of stiffening used in this study was far more than would ever be used in any prosthetic replacement valve, this study serves as a proof of concept for tailoring valvular leaflets characteristics to individual patients in order to optimize the hemodynamics inside the ascending aorta. Furthermore, the recent development of reliable polymer tri-leaflet prosthetic valves will make the manufacturing of these patient-specific valves much simpler and realistic.

4.2 **Prosthetic Valve Hemodynamics**

Both aortic Prosthetic Valve sizing and valve mounting configuration play a large role on the hemodynamics inside the aorta, and primarily, the residence time inside the sinus bulge. Valve sizing impacts the flow in two distinct ways. First, it affects the formation number of the systolic jet entering the aorta. Larger diameter valves exhibit a larger GOA. Therefore, under similar conditions (same stroke volume and heart rate) a larger valve will have a lower velocity systolic jet than a smaller diameter valve, and thus, a lower formation number. This can also be thought of as larger valve injecting less vorticity into the aorta[11]. Figure 3.10 shows the range of formation numbers covered by the different valves in this study. None of the tested valves reached formation number of less than 4, which is the point vortex ring pinch-off occurs[18]. This indicates that the systolic jets from the valves did not create individual vortices and instead exhibited well developed trailing jets and secondary vortical structures behind the primary vortex. Increasing formation number leads to linearly increasing mixing measures (average and standard deviation of velocity) in the areas near the leaflets of the valves. Due to the geometry of the trileaflet valves, these areas were the most "open" and allowed for the flow in the ascending aorta to interact with the fluid near the leaflets more readily. Therefore, the steady increase of the two mixing criteria with increasing formation number is to be expected because as the formation number grows, more vorticity is added to the fluid in the aorta and the velocity of the systolic jet also increases. However, the formation number does not have as strong of an effect on the fluid situated between the posts of the valve and the sinus wall (figure 3.11). This relates to the second mechanism by which valve sizing affects the flow in the sinus. The second way that valve sizing affects the aortic hemodynamics is that larger valves will inherently take up more volume inside the sinus bulge and the gap between their posts and the side of the sinus wall will be smaller. These smaller gaps are more isolated from the flow inside the aorta and can form pockets where blood remains trapped. The geometrical confinement of the blood flow is similar to how thrombosis can occur on TAVR valve leaflets when they have undergone improper implantation[16,33]. It is clear that the mixing criteria both decrease as the gap distance decreases (3.12). Furthermore, the average velocity in this region is almost half of that in the region near the leaflets. However, the average velocity and velocity standard deviation does not necessarily show the critical threshold where mixing in the region between the posts and

the sinus wall becomes too low. This is where the dye measurements become relevant. The dye visualization falls under two main categories valve configurations that managed to clear the majority of the dye in a single cardiac cycle, and valve configurations that took more than one cycle to clear the dye from the area under the valve post. The inability for a valve to completely clear dye in a single cardiac cycle indicates a significantly long blood residence time and a higher risk of thrombosis formation[20]. Comparing which valves performed poorly in the dye experiments with how they performed with the PIV velocity measurements provides a preliminary threshold for determining what gap distances will be acceptable to avoid thrombotic risk. The 25 mm Tria valve performed the worst in the dye visualization experiments. Referencing figure 3.12, we see that the gap distance for this valve was 1.57 mm and that both of the mixing criteria were 0.01 m/s. The 25 mm Perimount valve had a smaller gap distance of 1.47 mm but performed better than the 25 mm Tria on both the mixing parameters and in the dye visualization experiments. This is most likely because of the valve's smaller gross effective area and, thus, larger formation number. However, the dye visualization shows how late in the cardiac cycle the dye is cleared which indicates that the valve may be barely able to adequately washout the sinus. In order to account for both formation number and gap distance, Figure 4.1 presents the mixing criteria between the post and the sinus wall against the product of the formation number and the ratio of the gap distance over the diameter of the valve. This ratio will be called the formation gap ratio.

It is important to clarify that 25 mm Tria valve is not an inherently poorly performing valve. As previously stated, the dimensions of the human sinus bulge vary from 27 mm to 36 mm, and the 25 mm Tria valve is an oversized configuration for the 32mm sinus bulge. This valve choice proved useful as a test case for studying detrimental effects of oversizing on a patient's health and to challenge the current trend for surgeons to use the largest prosthetic valve available (1.3.8). The 25 mm Tria valve would be an adequate choice in patients with larger sinus bulges as cardiac output and aortic root size tend to increase with increasing body surface area (BSA)[22,13].

The presence of Cor-Knots mounting posts around the valve also heavily influenced the residence time in the aorta. Three different valves were tested with and without Cor-Knots. These were the 21 mm Tria, the 23 mm Tria, and the 25 mm Perimount. Unfortunately, the 25 mm Tria could not be tested with Cor-knots because this configuration could not fit inside the glass sinus model. In their normal mounting configuration, all of the tested valve configurations managed to clear the dye after a single cycle. However, both the 23 mm Tria and the 25 mm Perimount exhibited significantly higher dye residence time when mounted with Cor-knots. This trend continued with the PIV measurements with all Cor-Knot mounted valves showing lower mixing criteria both near the leaflets and between the post and sinus wall. However, both the 23 mm Tria and the 25 mm Perimount valve recovered performance with higher cardiac outputs in the dye visualization and in mixing criteria in the gap between the post and sinus. This phenomenon indicates that the presence of Cor-knots pushes the 23 mm Tria and 25 mm Perimount past the critical threshold where their residence time becomes significant. Essentially, the Cor-Knots act as baffles to the flow that severely impedes flow. This decrease in mixing criteria was even present in the more open region of the valve near the leaflets. The 21 mm Tria did not exhibit a detrimental increase in dye residence time and maintained adequate mixing criteria for both cardiac outputs tests which implies that the 21 mm valve's large gap distance and high formation number could create adequate washout despite the effects of the Cor-Knots.

The work presented serves to highlight the importance of proper aortic valve sizing and to define a possible threshold for valve oversizing. There has been a trend among surgeons to implant the largest valve possible in order to minimize the transvalvular pressure drop and prevent patient prosthetic mismatch[9,14]. However, there has been very little previous work on the effects of valve oversizing. Our work shows how oversized valves can significantly reduce the washout around the different prosthetic aortic valves, especially when Cor-Knots are present around the valves. According to our observations, valves perform in a binary manner, where the valve either creates enough washout to present hemostasis between the posts and sinus wall or fluid remains after each cardiac cycle and increases the risk of thrombosis. The dominant factors that affect the propensity for a valve to perform poorly are

the valve's gap distance between the valve's post and the sinus wall and the systolic formation number. The gap distance is affected by the external size of the implanted valve and the size of the sinus bulge. Large valves implanted inside small sinuses will lead to tight spacing between the two, which could lead to reduced velocity and mixing in that area, increasing residence time. A valve's systolic formation number increases with increasing stroke volume and decreases with valve gross orifice area. In the future, proper valve sizing must balance patient prosthetic mismatch against valve oversizing. Larger valves that exhibit smaller and more favorable transvalvular gradients will also take up more space inside the sinus and risk small gap distances and lower formation numbers. This study also illustrates that a formation gap ratio of less than 0.5 puts the valve at risk of hemostasis and thrombosis. The presence of Cor-knots further exacerbates the risks and increase blood residence time. These devices should be investigated further to ascertain the degree to which they effect the hemodynamics inside the aorta and to weigh the benefits they provide versus the risks they introduce. Future work must be done in order to validate these findings inside an *in vivo* model. However, formation gap ratio can be readily measured through pre-operative imaging and could provide surgeons with a necessary upper bound for valve sizing.

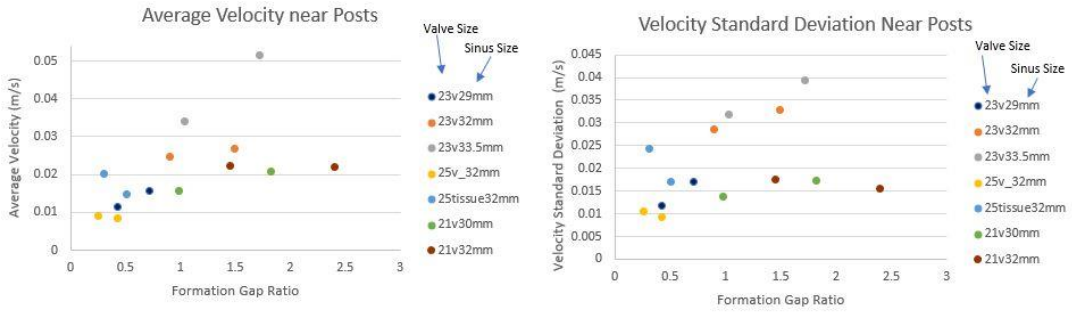

Figure 4.1: Mixing metrics plotted against Formation Gap Ratio for all valves without Cor-Knots.

4.3 **Study Limitations**

The aforementioned work was carried out in a vascular glass model. While useful for identifying trends that stenotic valves would produce inside the human vasculature, there are several limitations inherent to this *in vitro* experimental setup. First, the material properties of the glass aorta analog prevented the model's walls from exhibiting the compliance of the human vasculature system. Previous studies have documented the effect of compliance on the hemodynamics inside the aorta. Most significantly to this work, rigid aorta models have higher systolic velocities and an increased amount of turbulent kinetic energy[5,21]. Furthermore, a compliant aorta model would likely change how WSS, and wall-normal stress are distributed along the wall as the vessel deforms due to these stresses. We deemed the need for image clarity to be more important for this initial work because movement of the aortic wall would degrade our measurement and analysis of the WSS. Moreover, we feel that the relative differences that were described in the native valve study, such as the ability for stenotic valves to divert the systolic jet into the aortic wall, will hold in compliant models that will be carried out in future works. Secondly, velocity information was only measured from within a 2-dimensional cross-section of the flow. This prevented us from measuring the complex out of plane flow patterns which make up the hemodynamics inside the aorta. However, we were most interested in the flow patterns that were in the same plane as the aortic arch. Third, our system for creating non-uniform stiffness conditions for different stenotic native valve configurations was binary, as in each leaflet was either unstiffened or stiffened. We did not investigate the effect of different levels of stiffness for each leaflet. Our goal was to measure the maximal effect that non-uniform leaflet stiffness conditions could produce. However, it is unlikely that entire leaflets would be stiffened uniformly as seen in this work. Calcium deposits and fibrosis can semi-randomly accumulate on the leaflet's surface meaning that the stiffness of a single leaflet can vary wildly. We deemed that this added to much variability and was excluded from our model but would be interesting to future work. Furthermore, our experiment still identifies very informative trends about the effects that AS can have inside the aorta. Fourth, our method for measuring wall shear stress was an estimate that could only be used to measure the relative level of wall shear stress between different valve configurations. This limitation arises from the difficulty in measuring near-wall velocity gradients accurately. However, the relative measurements

described above are useful for understanding the effect that different valve configurations have on the hemodynamics near the wall. Finally, the 2-dimensional nature of the laser sheet, coupled with the complex geometry of the Cor-Knots made it impossible to measure velocity and residence time information behind individual Cor-Knots. Future work will have to be performed to study this area as it would be expected that the flow there would be very susceptible to thrombus formation.

BIBLIOGRAPHY

1. Barker, Alex J., et al. “Bicuspid Aortic Valve Is Associated with Altered Wall Shear Stress in the Ascending Aorta.” Circulation: Cardiovascular Imaging, vol. 5, no. 4, 2012, pp. 457–466., doi:10.1161/circimaging.112.973370.

2. Betts, J. Gordon, et al. Anatomy and Physiology. OpenStax College, Rice University, 2013.

3. Bonow, Robert O., et al. “2008 Focused Update Incorporated into the ACC/AHA 2006 Guidelines for the Management of Patients with Valvular Heart Disease.” Circulation, vol. 118, no. 15, 2008, doi:10.1161/circulationaha.108.190748

4. Bosi, Giorgia M., et al. “Population-Specific Material Properties of the Implantation Site for Transcatheter Aortic Valve Replacement Finite Element Simulations.” Journal of Biomechanics, vol. 71, 2018, pp. 236–244., doi:10.1016/j.jbiomech.2018.02.017

5. Büsen, Martin, et al. “Development of an in Vitro PIV Setup for Preliminary Investigation of the Effects of Aortic Compliance on Flow Patterns and Hemodynamics.” Cardiovascular Engineering and Technology, vol. 8, no. 3, 2017, pp. 368–377., doi:10.1007/s13239-017-0309-y

6. Cannegieter, S C, et al. “Thromboembolic and Bleeding Complications in Patients with Mechanical Heart Valve Prostheses.” Circulation, vol. 89, no. 2, Feb. 1994, pp. 635–641., doi:10.1161/01.cir.89.2.635

7. Cerillo, Alfredo Giuseppe, et al. “Increased Gradients after Aortic Valve Replacement with the Perceval Valve: The Role of Oversizing.” The Annals of Thoracic Surgery, vol. 106, no. 1, 2018, pp. 121–128., doi:10.1016/j.athoracsur.2017.12.044

8. Chambers, J. "Prosthetic Heart Valves." International Journal of Clinical Practice 68.10 (2014): 1227-230. https://doi.org/10.1111/ijcp.12309

9. Cleveland, John D., et al. “Evaluation of Hemodynamic Performance of Aortic Valve Bioprostheses in a Model of Oversizing.” The Annals of Thoracic Surgery, vol. 103, no. 6, 2017, pp. 1866–1876., doi:10.1016/j.athoracsur.2016.10.019.

10. Cunningham, Kristopher S, and Avrum I Gotlieb. “The Role of Shear Stress in the Pathogenesis of Atherosclerosis.” Laboratory Investigation, vol. 85, no. 1, 2004, pp. 9–23., doi:10.1038/labinvest.3700215

11. Dabiri, John O. “Optimal Vortex Formation as a Unifying Principle in Biological Propulsion.” Annual Review of Fluid Mechanics, vol. 41, no. 1, 2009, pp. 17–33., doi:10.1146/annurev.fluid.010908.165232

12. Dangas, George D., et al. “Prosthetic Heart Valve Thrombosis.” Journal of the American College of Cardiology, vol. 68, no. 24, 2016, pp. 2670–2689., doi:10.1016/j.jacc.2016.09.958

13. Devereux, Richard B et al. “Normal limits in relation to age, body size and gender of two-dimensional echocardiographic aortic root dimensions in persons ≥15 years of age.” The American journal of cardiology vol. 110,8 (2012): 1189-94. doi:10.1016/j.amjcard.2012.05.063

14. Dumesnil, J.G., and A.P. Yoganathan. “Valve Prosthesis Hemodynamics and the Problem of High Transprosthetic Pressure Gradients.” European Journal of Cardio-Thoracic Surgery, vol. 6, no. Supplement_1, 1992, doi:10.1093/ejcts/6.supplement_1.s34.

15. Dumesnil, J.G., Pibarot, P. Prosthesis-Patient Mismatch: An Update. Curr Cardiol Rep 13, 250–257 (2011). https://doi.org/10.1007/s11886-011-0172-7

16. Farhan Khodaee, Mohammed Barakat, Mostafa Abbasi, Danny Dvir, Ali N Azadani, Incomplete expansion of transcatheter aortic valves is associated with propensity for valve thrombosis, Interactive CardioVascular and Thoracic Surgery, Volume 30, Issue 1, January 2020, Pages 39–46, https://doi.org/10.1093/icvts/ivz213

17. Fung, Y. C. Biodynamics: Circulation. Springer, 1984.

18. Gharib,Morteza, et al. “A Universal Time Scale for Vortex Ring Formation.” Journal of Fluid Mechanics, vol. 360, 1998, pp. 121–140., doi:10.1017/s0022112097008410

19. Gharib, Morteza, et al. “Optimal Vortex Formation as an Index of Cardiac Health.” Proceedings of the National Academy of Sciences, vol. 103, no. 16, 2006, pp. 6305–6308., doi:10.1073/pnas.0600520103.

20. Groves, Elliott M et al. “The effects of positioning of transcatheter aortic valves on fluid dynamics of the aortic root.” ASAIO journal (American Society for Artificial Internal Organs : 1992) vol. 60,5 (2014): 545-552. doi:10.1097/MAT.0000000000000107

21. Gulan, Utku, et al. “Experimental Investigation of the Influence of the Aortic Stiffness on Hemodynamics in the Ascending Aorta.” IEEE Journal of Biomedical and Health Informatics, vol. 18, no. 6, 2014, pp. 1775–1780., doi:10.1109/jbhi.2014.2322934

22. Jegier, W., et al. “The Relation between Cardiac Output and Body Size.” Heart, vol. 25, no. 4, 1963, pp. 425–430., doi:10.1136/hrt.25.4.425

23. Jenkin, Ifan, et al. “The Role of Cor-Knot in the Future of Cardiac Surgery: A Systematic Review.” Journal of Cardiac Surgery, vol. 35, no. 11, 2020, pp. 2987–2994., doi:10.1111/jocs.14953

24. Jenney, Chris, et al. “Assessment of a Siloxane Poly(Urethane-Urea) Elastomer Designed for Implantable Heart Valve Leaflets.” Advanced NanoBiomed Research, vol. 1, no. 2, 2020, p. 2000032., doi:10.1002/anbr.202000032

25. Jhun, Choon-Sik, et al. “Dynamics of Blood Flows in Aortic Stenosis: Mild, Moderate, and Severe.” ASAIO Journal, vol. 67, no. 6, 2020, pp. 666–674., doi:10.1097/mat.0000000000001296

26. Johansen, Peter. “Mechanical Heart Valve Cavitation.” Expert Review of Medical Devices, vol. 1, no. 1, 2004, pp. 95–104., doi.org/10.1586/17434440.1.1.95

27. Johnston, I D, et al. “Mechanical Characterization of Bulk Sylgard 184 for Microfluidics and Microengineering.” Journal of Micromechanics and Microengineering, vol. 24, no. 3, 2014, p. 035017., doi:10.1088/0960-1317/24/3/035017

28. Kheradvar, Arash, et al. “Correlation between Vortex Ring Formation and Mitral Annulus Dynamics during Ventricular Rapid Filling.” ASAIO Journal, vol. 53, no. 1, 2007, pp. 8–16., doi:10.1097/01.mat.0000249870.44625.22

29. Kheradvar, A., Groves, E.M., Goergen, C.J. et al. “Emerging Trends in Heart Valve Engineering: Part II. Novel and Standard Technologies for Aortic Valve Replacement.” Ann Biomed Eng 43, 844–857 (2015). https://doi.org/10.1007/s10439-014-1191-51.3.3.1-3

30. Von Knobelsdorff-Brenkenhoff, Florian, et al. “Evaluation of Aortic Blood Flow and Wall Shear Stress in Aortic Stenosis and Its Association with Left Ventricular Remodeling.” Circulation: Cardiovascular Imaging, vol. 9, no. 3, 2016, doi:10.1161/circimaging.115.004038.

31. Li, Qianhui, et al. “Comparative Study of Wall-Shear Stress at the Ascending Aorta for Different Mechanical Heart Valve Prostheses.” Journal of Biomechanical Engineering, vol. 142, no. 1, 2019, doi:10.1115/1.4043357

32. Luthra, Suvitesh, et al. “Impact of Valve Size, Predicted Effective and Indexed Effective Orifice Area after Aortic Valve Replacement.” Journal of Cardiac Surgery, vol. 36, no. 3, 2021, pp. 961–968., doi:10.1111/jocs.15311

33. Makkar, Raj R., et al. “Possible Subclinical Leaflet Thrombosis in Bioprosthetic Aortic Valves.” New England Journal of Medicine, vol. 373, no. 21, 2015, pp. 2015–2024., doi:10.1056/nejmoa1509233

34. Maragiannis, Dimitrios, et al. “Replicating Patient-Specific Severe Aortic Valve Stenosis with Functional 3D Modeling.” Circulation: Cardiovascular Imaging, vol. 8, no. 10, 2015, doi:10.1161/circimaging.115.003626

35. Marquis-Gravel, Guillaume, et al. “Medical Treatment of Aortic Stenosis.” Circulation, vol. 134, no. 22, 2016, pp. 1766–1784., doi:10.1161/circulationaha.116.023997

36. Nagamine, Hiroshi, et al. "Ascending Aortic Aneurysm Exposed to Direct Impingement of Eccentric Flow Jets through a Tilting-Disc Valve Prosthesis." Journal of Surgical Case Reports, vol. 2019, no. 5, 2019, doi:10.1093/jscr/rjz127

37. Nathaniel, Sangeetha. "Aortic Stenosis: An Update." World Journal of Cardiology, vol. 2, no. 6, 2010, p. 135., doi:10.4330/wjc.v2.i6.135

38. Van Ooij, Pim, et al. "Aortic Valve Stenosis Alters Expression of Regional Aortic Wall Shear Stress: New Insights from a 4-Dimensional Flow Magnetic Resonance Imaging Study of 571 Subjects." Journal of the American Heart Association, vol. 6, no. 9, 2017, doi:10.1161/jaha.117.005959

39. Pham, Thuy, and Wei Sun. "Material Properties of Aged Human Mitral Valve Leaflets." Journal of Biomedical Materials Research Part A, vol. 102, no. 8, 2013, pp. 2692–2703., doi:10.1002/jbm.a.34939

40. Pibarot, Philippe, and Jean G Dumesnil. "Hemodynamic and Clinical Impact of Prosthesis–Patient Mismatch in the Aortic Valve Position and Its Prevention." Journal of the American College of Cardiology, vol. 36, no. 4, 2000, pp. 1131–1141., doi:10.1016/s0735-1097(00)00859-7

41. Shaw, Peter. "Faculty of 1000 Evaluation for NIH Image to Imagej: 25 Years of Image Analysis." F1000 - Post-Publication Peer Review of the Biomedical Literature, 2012, doi:10.3410/f.717951500.793456800

42. Sievers, Hans-Hinrich, and Hans Lennard Sievers. "Aortopathy in Bicuspid Aortic Valve Disease — Genes or Hemodynamics? or Scylla and Charybdis?" European Journal of Cardio-Thoracic Surgery, vol. 39, no. 6, 2011, pp. 803–804., doi:10.1016/j.ejcts.2011.02.007

43. Sommers, K.Eric, and Tirone E David. "Aortic Valve Replacement with Patch Enlargement of the Aortic Annulus." The Annals of Thoracic Surgery, vol. 63, no. 6, 1997, pp. 1608–1612., doi:10.1016/s0003-4975(97)00127-6

44. Sotiropoulos, F., Borazjani, I. A review of state-of-the-art numerical methods for simulating flow through mechanical heart valves. Med Biol Eng Comput 47, 245–256 (2009). https://doi.org/10.1007/s11517-009-0438-z

45. Thielicke, William, and Eize J. Stamhuis. "PIVlab – towards User-Friendly, Affordable and Accurate Digital Particle Image Velocimetry in Matlab." Journal of Open Research Software, vol. 2, 2014, doi:10.5334/jors.bl.

46. Vahidkhah, Koohyar, and Ali N. Azadani. "Supra-Annular Valve-in-Valve Implantation Reduces Blood Stasis on the Transcatheter Aortic Valve Leaflets." Journal of Biomechanics, vol. 58, 2017, pp. 114–122., doi:10.1016/j.jbiomech.2017.04.020.

47. Vahidkhah, Koohyar, et al. “Flow-Induced Damage to Blood Cells in Aortic Valve Stenosis.” Annals of Biomedical Engineering, vol. 44, no. 9, 2016, pp. 2724–2736., doi:10.1007/s10439-016-1577-7.

48. Willert, C. E., and M. Gharib. “Digital Particle Image Velocimetry.” Experiments in Fluids, vol. 10, no. 4, 1991, pp. 181–193., doi:10.1007/bf00190388.

49. Yousif, M.Y., Holdsworth, D.W. & Poepping, T.L. A blood-mimicking fluid for particle image velocimetry with silicone vascular models. Exp Fluids 50, 769–774 (2011). https://doi.org/10.1007/s00348-010-0958-1

Appendix A:

Stenotic Valve Systolic Jet Time Sequences

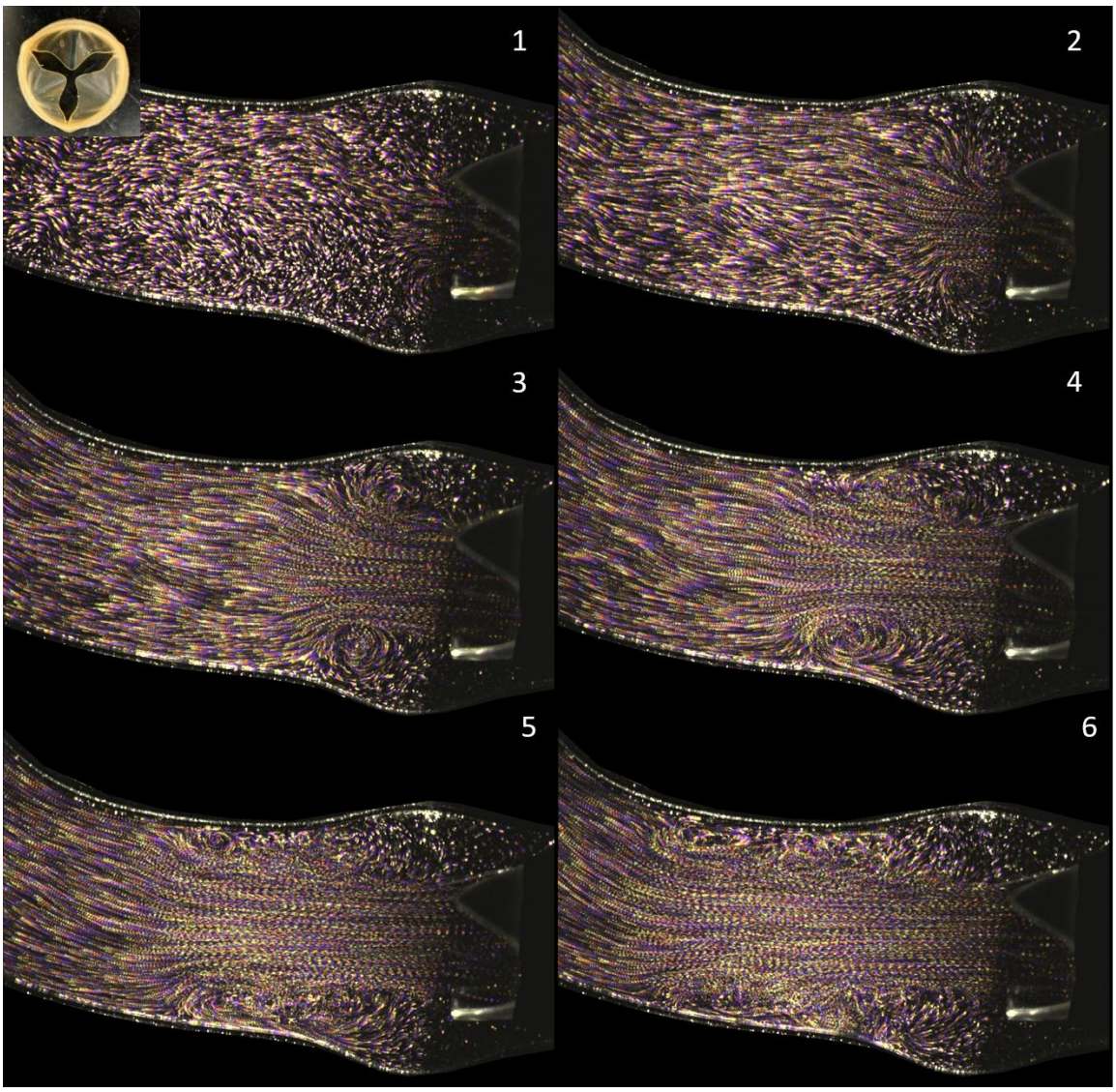

Figure A-1: Time evolution of the systolic jet in the ST (symmetric typical) configuration. In each case, the spacing between each image in a sequence was held constant such that the first image was captured at 8.333% of the systolic cycle, the second image was at the 16.667%, the third was at 25%, the fourth was at 33.333%, the fifth was at 41.667%, and the sixth was at 53%. This scheme is identical for figures A.1-A.4.

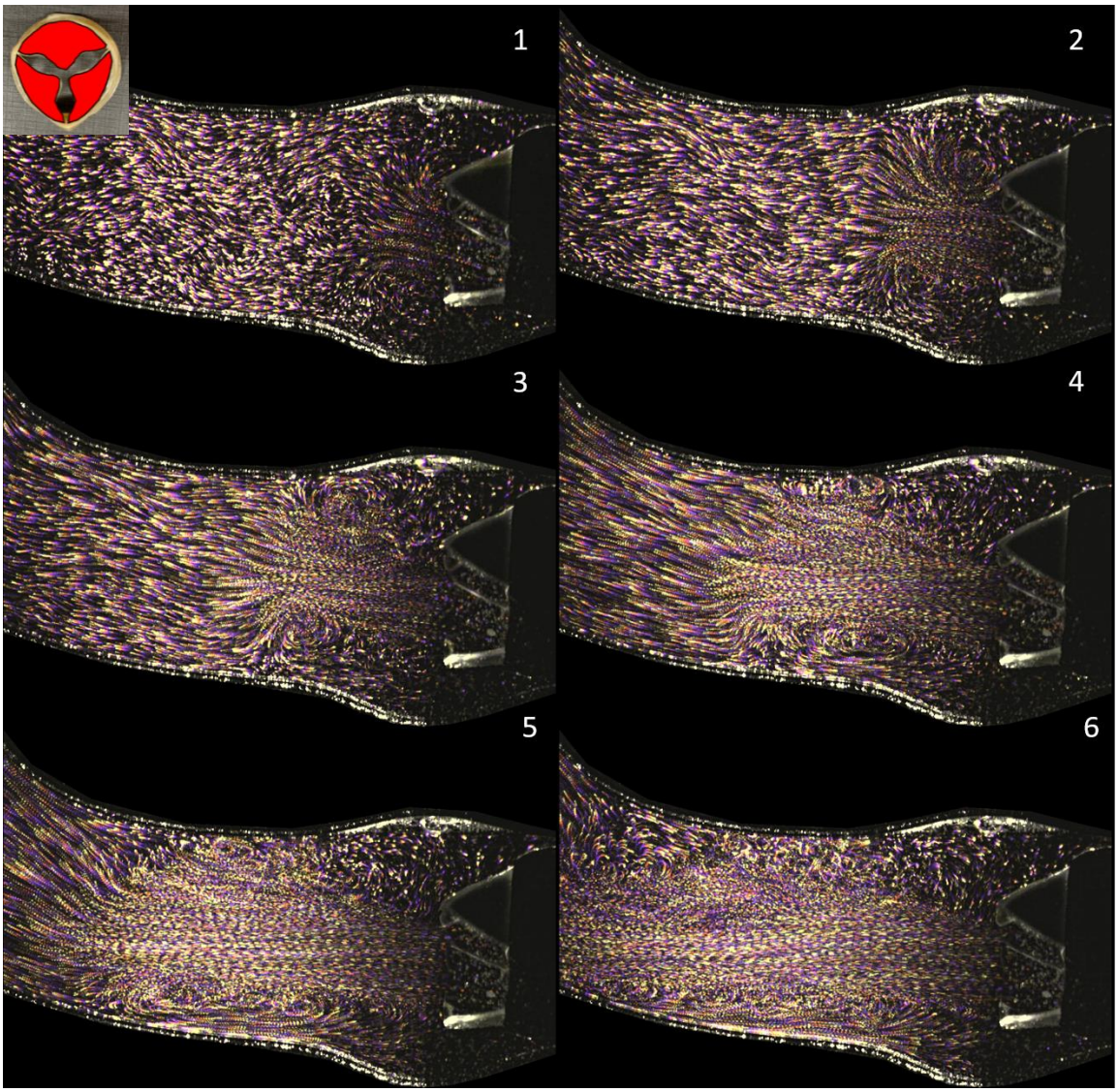

Figure A-2: Time evolution of the systolic jet in the SS (symmetric stenotic) configuration

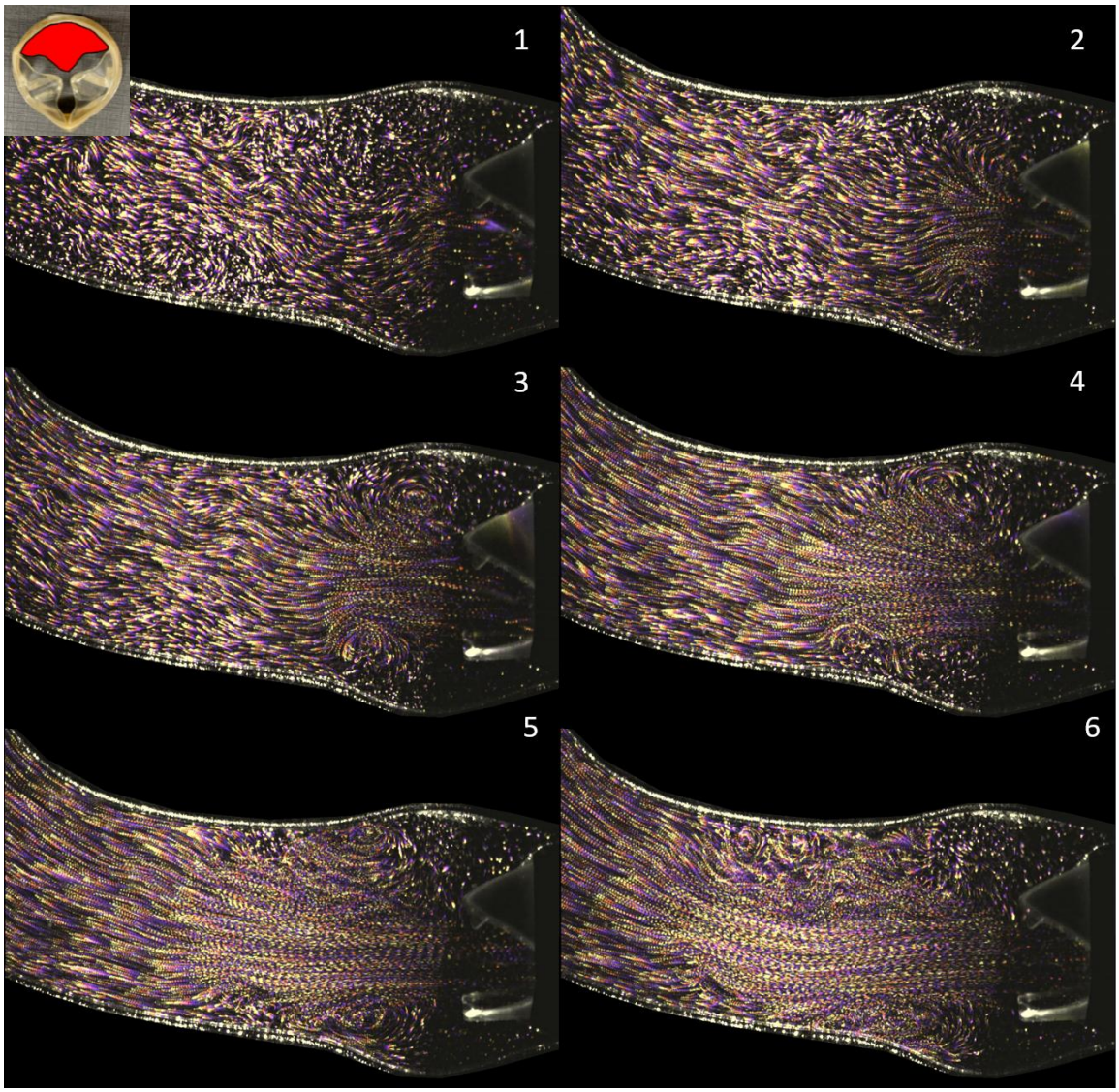

Figure A-3: Time evolution of the systolic jet in the A1 (asymmetric 1) configuration.

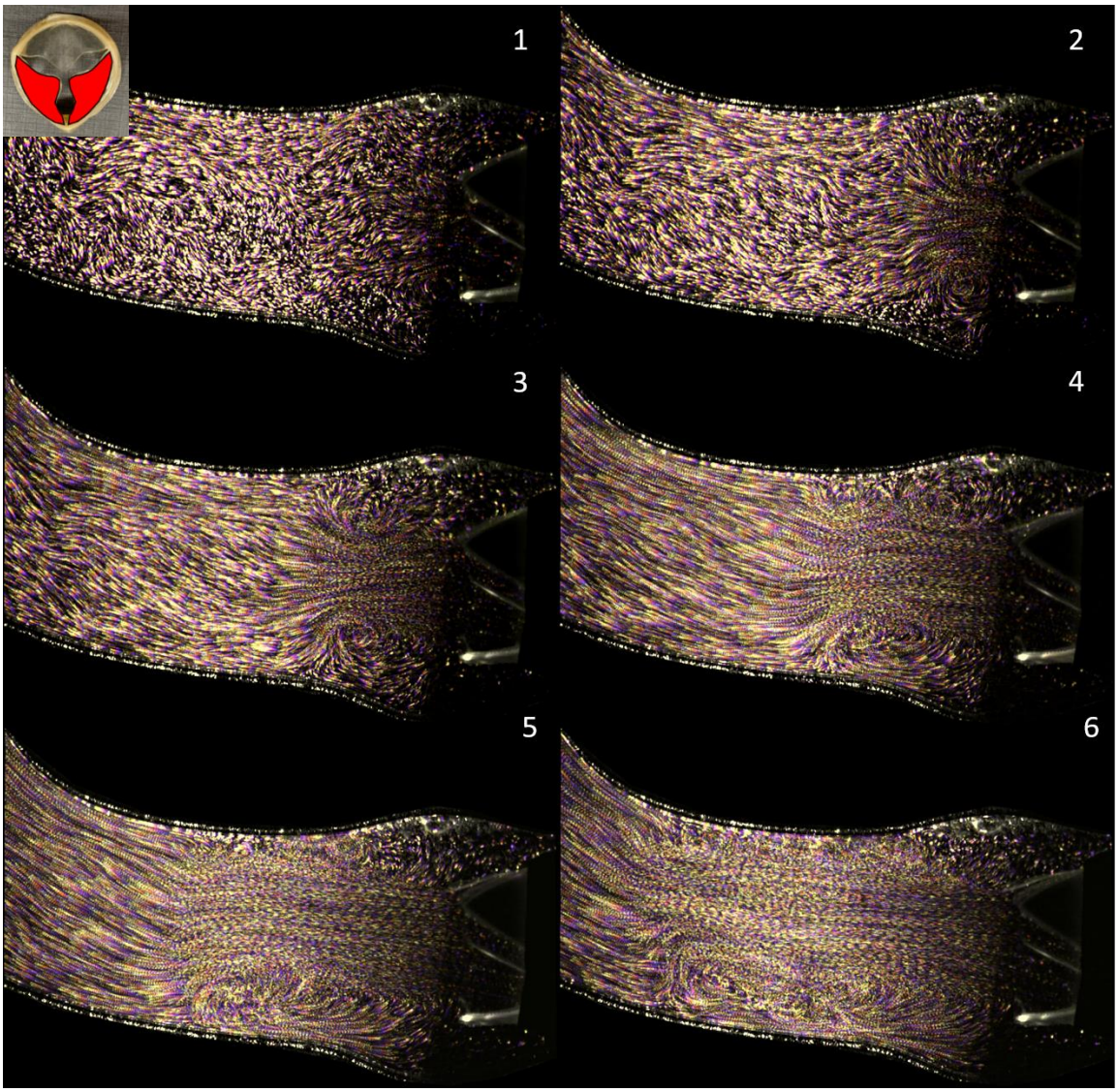

Figure A-4: Time evolution of the systolic jet in the A2 (asymmetric 2) configuration